View metadata, citation and similar papers at core.ac.uk
brought to you by CORE
provided by Universidade de Lisboa: Repositório.UL

UNIVERSIDADE DE LISBOA
FACULDADE DE CIÊNCIAS
DEPARTAMENTO DE ENGENHARIA GEOGRÁFICA, GEOFÍSICA E ENERGIA

Layout and modeling of a high temperature heat storage system for continuous operation of solar reforming processes

Pedro Miguel Boim Esteves Alves Roda

Dissertação

Mestrado Integrado em Engenharia da Energia e do Ambiente

2014

UNIVERSIDADE DE LISBOA
FACULDADE DE CIÊNCIAS
DEPARTAMENTO DE ENGENHARIA GEOGRÁFICA, GEOFÍSICA E ENERGIA

Layout and modeling of a high temperature heat storage system for continuous operation of solar reforming processes

Pedro Miguel Boim Esteves Alves Roda

Dissertação de Mestrado em Engenharia da Energia e do Ambiente

Trabalho realizado sob a supervisão de

Henrik von Storch (DLR)

Professor Guilherme Carrilho da Graça (FCUL)

2014

Acknowledgements

I would like to thank my supervisor Prof. Guilherme Carrilho da Graça and my co-supervisor Henrik von Storch all the support that they gave along my work.

In particularly, I would like to thank to Henrik von Storch for the entire time spent helping, teaching and guiding me on my thesis.

I also would like to thank to DLR (German aerospace center) to provide all the resources needed to my work and to thank to DLR's collaborators to receive me as one of them. Also my thanks to the Science's Faculty from the Univesity of Lisbon for giving me the chance to study abroad and fulfill my expectations as a student.

Also would like to thank my parents and siblings that helped trough all my academic life and made possible for me to achieve this moment.

Also my most sincerely thanks to all my friends, in particular, Leonardo Roda, Gonçalo Nunes and Mário Silva that always gave me the best advises and made me be a better person.

And at last but not least, the most important thanks to my girlfriend, Ana Tostão that helped me and dealt with me for my whole academic life without giving up.

Abstract

This thesis comprises a model of a high temperature heat storage system, modelled in Aspen Custom Modeler®, to be implemented in a solar methane reforming plant model. The model is a 1D approximation and does not consider thermal losses. The pressure drop along the system is considered as well as the temperature dependency of the fluid properties. The system modeled is a sensible heat storage system and uses alumina ceramic honeycombs as storage material.

The implementation of the storage system in a solar methane reforming plant will make possible to reduce the size of the plant, increase the operating period of the plant and achieve a constant annual output of the plant.

The thesis also presents a short state of the art in heat storage systems. The main objective of the thesis is to model the heat storage system to be implemented in a continuous operation simulation and also determine a relation between the layout of the system and the operating time of the plant.

Resumo

Esta tese contém um modelo de um sistema de armazenamento térmico de alta temperatura, o software usado para criar o modelo foi Aspen Custom Modeler®, que será implementado num modelo de uma central de reformação solar de metano. O modelo é uma aproximação unidimensional e as perdas térmicas são desprezadas. A variação da pressão e as propriedades dependentes da temperatura são consideradas neste modelo. O sistema modelado é um sistema capaz de armazenar calor sob a forma de calor sensível usando cerâmica alumina como material armazenador.

A implementação deste sistema numa central de reformação solar de metano irá permitir a redução do tamanho da central, permite aumentar as horas em operação ao longo do ano e permite que a central opere com um output constante durante todo o período em operação.

Esta tese apresenta ainda um pequeno estudo do estado da tecnologia em sistema de armazenamento térmico. O principal objectivo da tese é a criação do modelo do sistema de armazenamento térmico em que permita a operação contínua durante a sua simulação. É também objectivo deste trabalho apresentar uma relação entre o dimensionamento do sistema (material necessário) e o período que a central opera.

Palavras-chave: Heat storage, High temperature storage modeling, solar reforming with storage

Index

List of Figures

List of Tables

Nomenclature	**Description**	**Units**
Nu	Nusselt number	
Re	Reynolds number	
Pr	Prandtl number	
S	Air channel opening	M
L	Air channel length	M
n_{air}	Air flow	$Kmol.s^{-1}$
$c_{p,air}$	Air heat capacity	$kJ.(kmol^{-1}.K^{-1})$
$Tair$	Air temperature	°C
λ_{air}	Air conductivity	$W.(m^{-1}.K^{-1})$
ρ_{air}	Air density	$kmol.m^{-3}$
$A_{cs,air}$	Air channel cross section	m^2
h_{air}	Air enthalpy	$kJ.kmol^{-1}$
λ_{sol}	Ceramic conductivity	$W.(m^{-1}.K^{-1})$
ρ_{sol}	Ceramic density	$kg.m^{-3}$
$C_{p,sol}$	Ceramic heat capacity	$kJ.(kg^{-1}.K^{-1})$
$A_{cs,sol}$	Ceramic cross section	m^2
T_{sol}	Ceramic Temperature	°C
α	Convection heat transfer coefficient between air and ceramic	$W.(m^{-2}.K^{-1})$
$Q_{st,wall}$	Energy stored in the solid	kJ
Q_{air}	Enthalpy air variation	kJ
$\dot{Q}_{to,storage}$	Energy available to store	$kJ.h^{-1}$
$Q_{Storage}(t+\Delta t)$	Energy stored	kJ
Δp	Pressure drop	bar
f	Friction factor	
D	Hydraulic diameter	m
V_{air}	Air velocity	$m.s^{-1}$
T_i	Initial temperature	K
T_m	Melting temperature	K
m	Mass of heat storage medium	Kg
a_m	Fraction melted	
Δh_m	Heat of fusion per unit mass	$J.kg^{-1}$

Abbreviations	
CSP	Concentrating Solar thermal Power
HTF	Heat transfer Fluid
LEC	Levelised Electricity cost
EPC	Engineering, procurement and construction
O&M	Operation and maintenance
SMR	Steam methane reforming
DMR	Dry methane reforming
STJ	Solar Tower Jülich

1. Introduction

It is a fact that the fossil fuels resources are limited around the world. Due to that limitation and also their harmful contribute to the humanity and climate, greatly because of their CO_2 emissions, the is experiencing an increasing usage of renewable energy sources (Müller-Steinhagen and Trieb 2004). Governments and companies all over the world are turning their own mind-set to a more sustainable future with incentives to reduce their foot print and the so called "green economy".

A transition between a fossil fuel based, mature and well known grid to a renewable based grid cannot be an abrupt process. When renewable energy resources are added to the grid, they bring with them instability and fluctuation which reduces the feasibility and quality of the grid. There are already a couple of renewable energy technologies in a higher level of maturation, like PV and wind power, which enables them to be the renewable energy technologies with most installed capacity worldwide (Trieb, Fichter et al. 2014). Even with PV and wind power with already being integrated in the grid, there is still a problem of transportation because usually the high sun rich (or wind rich) regions are not necessarily the regions with high energy demand.

A lot of researchers and research centres are putting their effort on studying concentrating solar technologies in order to integrate this technology in the grid in a near future, like any other renewable energy source, concentrating solar plants are instable and also like other solar technologies it is intermittent. This intermittency represents the biggest challenge to this technology, although there is a possibility to integrate a thermal storage system to these solar plants which could increase the working hours of these solar plants and also could make this technology more versatile and make use of the energy produced in periods with a higher energy demand (Nagl, Fürsch et al. 2011).

Concentrating solar plants are also being studied by researchers that believe that it can be a solution for the transportation drawback. Their investigations show that these plants could be used as an heat source for a gas reforming process which would produce fuels with an high heat capacity and lower CO_2 emissions when in combustion, these fuels are usually called solar fuels (Storch, Roeb et al. 2014). Solar energy will become a competitive technology as soon as this challenges are overcome (Yang, Du et al. 2013).

This thesis gives a short introduction to concentrating solar plants and technologies, a state of the art in thermal storage systems and an introduction to the solar methane reforming process.

The objective of the thesis is to create model a thermal storage system to be implemented in a model of a solar methane reforming plant for continuous operation and also determine the relation between storage material needed and working hours of the plant.

1.1 Concentrating solar principles

The most common way for producing electricity is to make use of a water/steam cycle. On a traditional fossil fuelled plant the fuel is combusted, the heat produced is used to boil water and produce steam that will spin a turbine and generate electricity. In concentrating solar plants (CSP) the high temperature heat will be achieved with solar radiation. Solar radiation collectors, usually mirrors, redirect and concentrate the solar radiation into a point or line, depending on the technology. This radiation focused in the heat exchanger will increase its temperature. Then a heat transfer fluid (HTF) will flow along the heat exchanger and will be used to heat up water, produce steam and generate electricity as in a conventional fossil fuelled plant (Pitz-Paal, Buck et al. 2013).

Unlike PV, that can make use of diffuse solar radiation, CSP can only make use of direct solar radiation. Two different principles, based on mirror's shape, are distinguished parabolic principle and Fresnel principle (Vogel and Kalb (April 2010):

1.1.1 Concentrating solar technologies

CSP makes use of lenses or mirrors to concentrate direct solar radiation into a point or line. Depending on technology the concentration factors can be from 50 to thousands (Pitz-Paal, Buck et al. 2013). The technologies differ in configuration, mirror's size and shape and application.

- **Dish plants**

  This technology makes use of a paraboloid dish mirror to reach the highest concentration factors in the range of 1000 - 3000. Due to the tracking system of this technology the incident solar radiation in the dish is all redirected to the heat engine or receiver located in a higher central point. On bottom right of Fig. 1 can be seen a representative scheme of this technology.

- **Tower power plants**

  Large mirrors are distributed along a field and for an array, the mirrors are individually monitored and track the sun with the aid of a double axis tracking system and focus the solar radiation into a point on the top of the tower. In this technology the temperatures achieved in the receiver are from 600°C to 1200 °C (Vogel and Kalb April 2010). On top right of Fig. 1 can be seen a representative scheme of this technology.

- **Parabolic Trough**

  The mirrors are usually called "U-shaped". When assembled the parabolic trough plants look like a cylinder cut in a half with a smaller tube in the center. This smaller tube is the receiver of this technology, where the sunlight is focused. Due to the redirected radiation the tube is heated up and consequently heats up the HTF that is flowing inside. The maximum operation temperature reached until now is around 550°C and some researchers are investigating the production of steam directly inside the tube. (Vogel and Kalb April 2010). On top left of Fig. 1 can be seen a representative scheme of this technology.

- **Linear Fresnel plants**

  The mirrors are nearly planar and placed closed to the ground. The mirrors are distributed parallel to each other forming a line and focusing the solar radiation into a receiver that is facing the ground. The mirrors track the sun with the aid of a single axis tracking system (Vogel and Kalb April 2010). On bottom left of Fig. 1 can be seen a representative scheme of this technology.

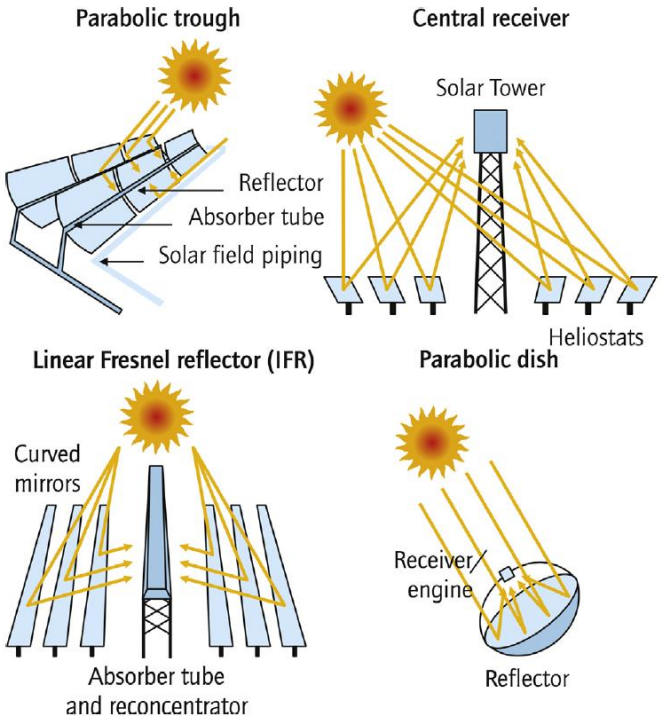

Fig. 1 - Technologies for concentrating solar radiation (Agrafiotis, von Storch et al. 2014).

1.1.2 CSP projects in Portugal

Portugal has a great potential to explore this type of technology. In this chapter are shown two CSP projects in Portugal.

- **SOLMASS project**

  This project will build a 4MW solar tower power plant, using a central receiver system. The plant will be constructed in Tavira, Algarve as development platform (Coelho, Domingues et al. 2010). This will be a hybrid unit and will use Biomass as backup. A layout of the hybrid unit can be seen in Fig. 2.

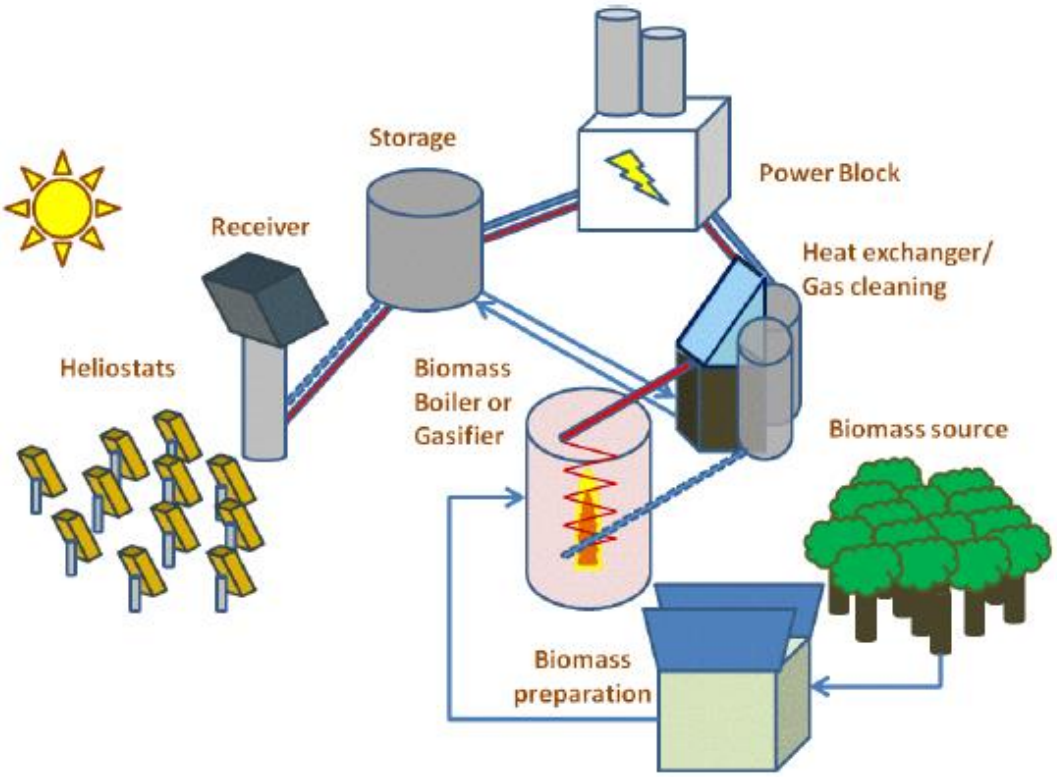

Fig. 2 - Hybrid unit layout to be built in Tavira by the SOLMASS project (Coelho, Domingues et al. 2010).

- **Parabolic salt loop project**

  The plant is of parabolic trough type and is already under construction in Évora, Portugal. The aim of the project is demonstrate the viability of this system using molten salt as alternative heat transfer fluid (Müller-Elvers, Wittmann et al. 2012).

1.2 Environmental Profile

It is mandatory to assess the environmental impacts of CSP and even if they are less when compared with conventional fossil fuelled technologies they cannot be neglected. It is a fact that CSP greenhouse gas emissions are lower than when compared with the same conventional plants, although the CSP impacts are local and can directly affected its surroundings. Some of them such as , water issues, land use, energy and materials use and emissions will be reviewed in the following points.

- **Water issues**

  In CSP water is used for cooling purposes. Also the places rich in sun and water usually are the most populated, which means that a rational usage of water should be made. An alternative to water is to use air as cooling medium but it will affect the efficiency of the process.

  Water in CSP is also used to keep the mirror cleaned and keep their reflective properties, although the amount of water used for cleaning purposes is much lower when compared with amount used for cooling.rect sunlight and hence are best constructed in arid or semi-arid regions, globally known as the Sun Belt.

  CSP are often designed to use water for cooling at the back-end of the thermal cycle, typically in a wet cooling tower. A typical 50MW parabolic trough plants uses 0.4 – 0.5 million m^3 of water per year for cooling. (European Academies Science Advisory Council 2011). Vogel and Kalb (April 2010) also show that the dry cooling system increases the

investment costs due to specific operating and maintenance costs of the system, the Solar Tower Jülich (STJ) is an example of a facility using this system.

- **Land use**

  Land use is the total area occupied by all the structures that belong and are needed to keep the plant working. In a CSP technology, the collectors field is the structure that will require a bigger area, usually CSP are built in arid places that will have clear skies. And like any other energy technology it will also bring some visual effects on the nearer populations, even when CSP one technology that makes a relatively efficient usage of the land occupied when compared to other solar technologies (Tsoutsos, Frantzeskaki et al. 2005). Table 1 shows a comparison between energy conversion technologies and CSP. It is presented in relation to the energy generated annually by each plant (European Academies Science Advisory Council 2011).

Table 1- Land use comparison between energy conversion technologies (European Academies Science Advisory Council 2011).

	Land use [$m^2 \cdot (MWh^{-1} \cdot y^{-1})$]
Parabolic solar power, Spain	11
Solar tower power, Spain	17
Photovoltaic power plant, Germany	56 (photovoltaic power can also be placed on rooftops which corresponds zero land use)
Wind power	<5
Biomass plantation, France	550
Open-cast mining (lignite), Germany	60
High-voltage power transmission line across Europe	0.4

- **Energy and materials use**

  If a life cycle assessment is made of a CSP technology it is immediately noticed that the greenhouse gas emissions are much lower than in conventional fossil fuelled power plants, although there are still some emission associated with CSP. Most of these emissions are related to the really high material use of CSP such as steel, pipes, and mirrors and, if storage is implemented, the salts used as storage system.

  CSP greenhouse effects can increase if fuel backup is used, because this is the only situation that fuel is used in CSP technology (European Academies Science Advisory Council 2011) and, excepting these cases , no fuel is used in CSP plants.

1.3 Socio-Economic impacts

As it is mentioned before the impacts of CSP are mostly local, this is also true for socio economic impacts. CSP technology needs some employees with high know-how but also need cleaning teams and maintenance so the local market can benefit with the project. Also the construction materials, since they are ordinary construction materials such as steel or concrete, can be purchased in local providers. A lot of CSP projects are built in smaller towns or isolated places, the local population can benefit of an increase demand of ordinary goods and services.

CSP costs vary with technology but the solar field's costs represent the biggest cost of the project. There will be operation and maintenance costs and also costs with personnel. It is extremely difficult to make a comparison between conventional fossil fuelled power plants and renewable energy power plants. A usual methodology to compare costs of electricity generation between such technologies is to calculate the "levelised electricity cost" (LEC) which relates average annual capital and operating costs of the plant to the annual electricity production (European Academies Science Advisory Council 2011). Table 2 illustrates the costs of generating technologies in 2010 (European Academies Science Advisory Council 2011).

Table 2- Illustrative costs of generating technologies in 2010 (currency conversion 2010 $/€ = 0.755) (European Academies Science Advisory Council 2011).

Technology	LEC [€c·kWhe^{-1}]	Capacity [MW]	EPC cost [€·kWe^{-1}]	Cap. factor	Fuel costs [€c·kWhe^{-1}]	O&M$_{fix}$ [€·kW^{-1} · y^{-1}]	O&M$_{var}$ [€c·kWhe^{-1}]
CSP: 100 MW no storage (Arizona)	17.9	100	3542	0.28	0	48	0
Pulverised coal: 650MW: base-load	6.9	650	2391	0.90	2.9	27	0.3
Pulverised coal: 650MW: base-load	9.0	650	2391	0.57	2.9	27	0.3
Gas combined cycle mid-load	6.1	540	738	0.40	3.2	11	0.3
Wind on-shore: 100MW	8.5	100	1841	0.3	0	21	0
Wind off-shore: 400MW	15.3	400	4511	0.4	0	40	0
Photovoltaic: 150MW (Arizona)	21.2	150	3590	0.22	0	13	0

Analysing Table 2 it is easy to notice that there is a long way for renewable energy resources to become competitive in the energy market. Although, with so many incentives and with the aim of governments to turn fossil fuelled economies into clean energy economies. And with the aim of private investors to reduce their companies carbon foot print it is expected that a cost reduction by scaling up renewable energy projects and technology innovations, will turn renewable energy resources into a competitive option (European Academies Science Advisory Council 2011).

1.4 Reforming process

1.4.1 Hydrogen production and methane reforming

Hydrogen production it is a process that is already being studied for a long time. Hydrogen production is mostly made by converting a material with high contents of hydrogen (H_2), such as gasoline, ammonia, or methanol, into hydrogen rich flow. This hydrogen can be later used in recent technologies like fuel cells. s an energy carrier and as an important "raw material" in chemical industries and refineries.

Theoretically the hydrogen produced all around the world, nowadays, is produced by the catalytic reforming of methane technique. Different reactions can take place in methane reforming and two of them are: (1) steam methane reforming (SMR) and (2) CO_2 (or dry) methane reforming (DMR) (Agrafiotis, von Storch et al. 2014).

$$CH_4 + H_2O \rightarrow 3H_2 + CO \qquad \Delta H = +206 kJ/mol \tag{1}$$

$$CH_4 + CO_2 \rightarrow 2H_2 + 2CO \qquad \Delta H = +247 kJ/mol \tag{2}$$

Both reactions are endothermic which means that an heat source is needed so that the reactions can take place. (Agrafiotis, Von Storch et al. 2014). Currently the hydrogen produced from fossil fuels is used as a chemical in industrial processes.

The reforming process, as mentioned above, needs energy to occur. If solar energy (or any other renewable energy resource) is used the process becomes free of fossil fuels, and in this case, the production of solar fuels is achieved. The process takes place in a range of temperatures from 800 to 1000°C which also means that there are already CSP technologies that can fit in this range.

2. Thermal storage

Independently of the energy production technology it is a great advantage if the energy is coming from a versatile, dispatchable, technology. This property enables the technology to provide energy (almost) on demand. It is a fact that solar is a non-dispatchable technology and this represents one of the major challenges on solar technology.

In CSP there is the option to integrate a thermal heat storage system that could maintain the plant working during cloudy periods and, if the thermal storage capacity is big enough, during night periods. Currently a lot of the researchers effort is to improve this systems and find one that is feasible and do not compromise the efficiency of the process and do not increase the cost of the whole plant into extremely high values.

This chapter gives an overview on the different types of thermal storage concepts, classification and materials and their properties.

2.1 Thermal energy storage concepts

There are different concepts for thermal heat storage systems. Two groups can be identified, active and passive systems. And active storage systems can be independently identified as direct or indirect, This type of classification is independent of the system's storage material and physical storage (Gil, Medrano et al. 2010).

The decision on which type of technology will be used in a certain application depends on operation temperature, boundary conditions and development of the technology.

2.1.1 Active direct and indirect storage systems

An active direct storage system is a more difficult system to implement because in this system the storage material is also the heat transfer fluid, which means that is necessary to find a material that can be a good heat transfer fluid and a good storage material decreasing the options that can fit in both.

An indirect storage system usually makes use of two different materials, one is the heat transfer fluid and other one is the storage material and by pumping the heat transfer fluid through a heat exchanger it will heat up the storage material that is also being pumped. Usually this is a more complex system in terms of infrastructures because tanks are needed (Gil, Medrano et al. 2010). A scheme of these concepts can be seen in Fig. 3.

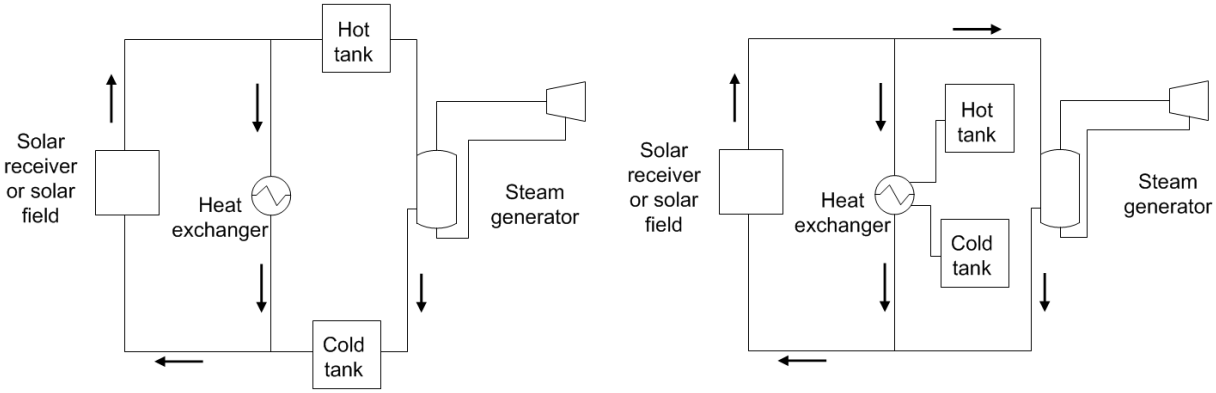

Fig. 3 - Scheme of active direct (left) and active indirect (right) storage systems.

2.1.2 Passive storage systems

In a passive storage system the heat transfer fluid will be pumped through another medium that will be the storage material, in this system the storage material is not being pumped and the heat transfer fluid is just used to charge or discharge the storage system (Gil, Medrano et al. 2010). A scheme of this storage concept can be seen in Fig. 4.

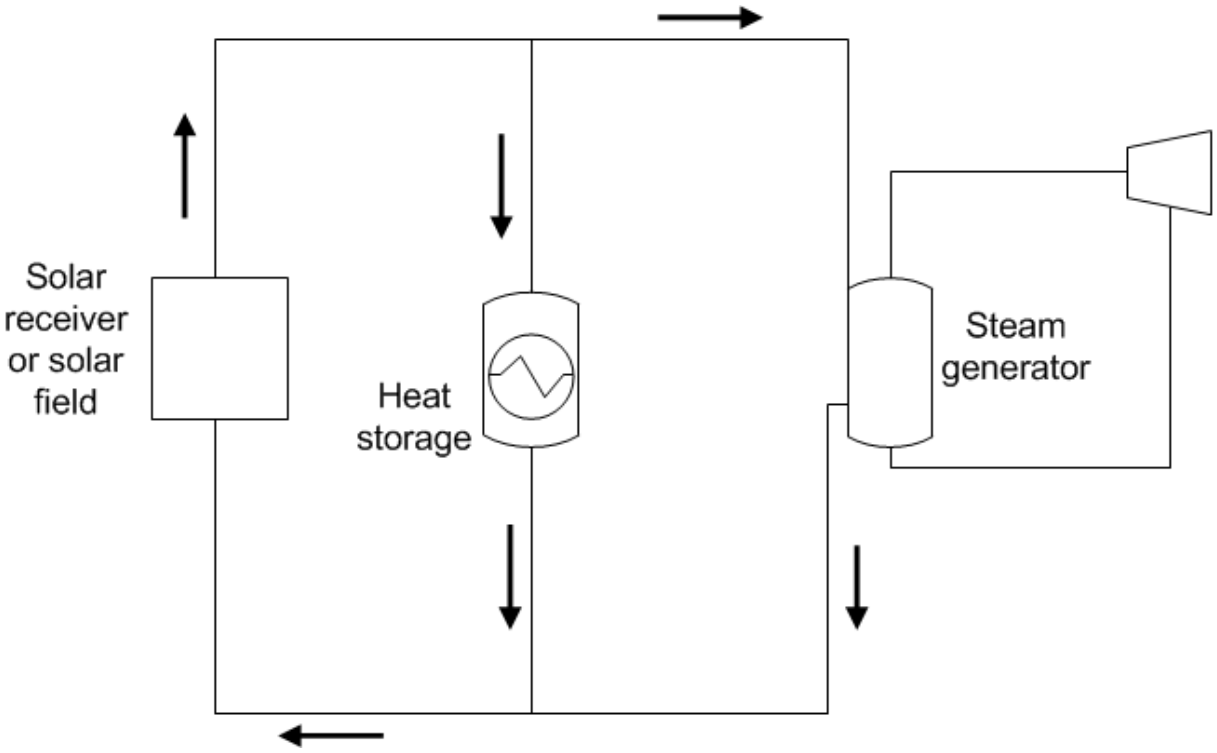

Fig. 4 - Scheme of a passive storage system.

The most common storage systems applied until now are the indirect storage system and the passive systems (or regenerators). On the next section there will be a detailed description about the storage medium and physical storage.

2.2 Storage Media

The storage system can have different storage media such as liquid, solid or gaseous the system can also make use of different physical phenomena to store energy by heating up a medium without phase change, making use of a phase change of a material at a certain temperature or by chemical reactions that are completely reversible.

On the following sections a detailed description on each storage media and some of their applications is presented.

2.2.1 Sensible Heat Storage

Sensible heat storage means that the energy will be stored in a material without its phase change. It is important to make a wise choice of material as well as an intensive study of its behavior under operating conditions. The material can be liquid, solid or gaseous and it will store energy accordingly with (3) (Hasnain 1998).

$$\Delta Q_{12} = m \int_{T_1}^{T_2} c_p(T) dT \tag{3}$$

2.2.1.1 Sensible heat storage materials

As it is mentioned above the storage material choice is a crucial point in heat storage systems. The material has to have desired properties for the application. And even when different physical heat storage will be presented, the storage materials will have a lot of properties in common. A list of desired properties of storage materials to be implemented in a sensible heat storage system are

presented below and categorized in thermo-physical-(A), chemical-(B), mechanical-(C), economic-(D), and environmental (E) properties (Khare, Dell'Amico et al. 2013):

(A)

- High energy density;
- High thermal conductivity;
- High heat capacity;
- High density;
- Long thermal cycling stability.

(B)

- Long thermal chemical stability with no chemical decomposition;
- Non-toxic;
- Non-explosive;
- Low corrosion potential or reactivity to heat transfer fluids;
- Compatible with materials of construction.

(C)

- Good mechanical stability;
- Low coefficient of thermal expansion;
- High fracture toughness;
- High compressive strength.

(D)

- Cheap and abundant materials;
- Low cost of manufacturing into suitable shapes.

(E)

- Low manufacturing energy requirement;
- Low CO_2 foot print.

After evaluating the properties requirements for a certain application a short list of materials should be elaborated and the materials should be intensively studied. Find if the material deteriorates under operating conditions, feasibility and thermal behavior. For high temperature applications the most promising materials are ceramics and metals (Khare, Dell'Amico et al. 2013).

2.2.1.2 Sensible heat storage concepts

The two main concepts of sensible heat storage systems are solid and liquids which will be explained in detail on the following points:

- **Solids**

  Chose a solid material as a storage the storage material is usually a choice based on its low cost. When solids are used, ordinarily concrete, leakages, phase changes, freezing or evaporation problems are not faced. On the other hand solids durability, degradation after several cycles of use and their low thermal conductivity represent the biggest disadvantages of this concept (Shukla 1981).

- **Liquids**

  Liquids have the high thermal conductivity as their big advantage but for high temperatures they have to be pressurized. Freezing and boiling points are the biggest challenges on sensible heat storage systems using liquids as storage material, which also makes it a more difficult storage material to store (Shukla 1981).

There are already few systems implemented, under investigation or in test campaigns. On the following sections some examples of both concepts are presented.

2.2.1.3 Examples of sensible heat storage systems

- **Concrete**

  Concrete is a tempting option since it is a relatively cheap material, it is widely use around the world and it is abundant.

  The systems using concrete as storage material consist of concrete block that is crossed by a tube matrix. The heat transfer fluid flows through the tubes and heats up the concrete block. This concept has already been tested and concrete showed a great durability performance. Although the system requires a huge area to be installed and its low thermal conductivity has to be improved, which represent the biggest disadvantages of the system.

  Thermal stability of concrete was evaluated but only for temperature ranges of 400 - 500°C. For this temperature ranges a concrete storage test module was built and tested in The system was tested in a temperature range between 400 - 500°C in Stuttgart, Germany (Laing, Bahl et al. 2012). A system sizing determination for the parabolic through solar thermal power plant of the ANDASOL-type was calculated and a 50000 m^3 is required and has to be built in a modular approach (Laing, Bahl et al. 2012).

  Some solutions for the poor thermal performance due to concrete's low thermal conductivity (range: 1.2 – 1.45 $W \cdot m^{-1} \cdot K^{-1}$) were investigated and an improvement of around 15% was achieved by adding structures with high thermal conductivity (Laing, Steinmann et al. 2008).

- **2 Tank molten Salt Indirect Storage**

  The two tank system is one of the most storage systems implemented. This system uses liquid as the storage media. This heat storage system consists of 2 tanks, one hot tank and one cold tank. During charging, the salt from the cold tank is pumped through the heat exchanger and is heated up by the heat transfer fluid and stored in the hot tank. During the discharging cycle the direction is reversed and the hot salt heats up the heat transfer fluid and is stored in the cold tank. If the heat transfer fluid is also used as storage material, the heat exchanger is not needed in the systems.

  This is system was successfully tested in the Solar Two project and its operating temperatures are between 290-390°C using a molten salt mixture. This system is always limited by the molten salt allowable operating temperatures because the mixture cannot freeze inside the tanks or pipes system it limits the lowest temperature. And since corrosivity increases with the temperature, for molten salts, tank's materials have to be chosen carefully. And the mixture's thermal performance can be affected in higher temperatures (Kolb 2011, Dunn, Hearps et al. 2012).

- **Steam accumulator**

  Steam accumulators systems are storage systems for short periods that solar radiation is not available, like cloudy periods since accumulators deliver the energy stored quickly, and its cost are proportional to the pressure vessel used in the system.

  Steam accumulators make use of the high water thermal conductivity property and since water is not liquid above 100°C, for CSP applications it has to be pressurized. The system

is charged by providing steam to the liquid medium of the steam accumulator that will increase the liquid water temperature. For discharging, the pressure is lowered and steam is generated. A scheme of this system is presented in Fig. 5.

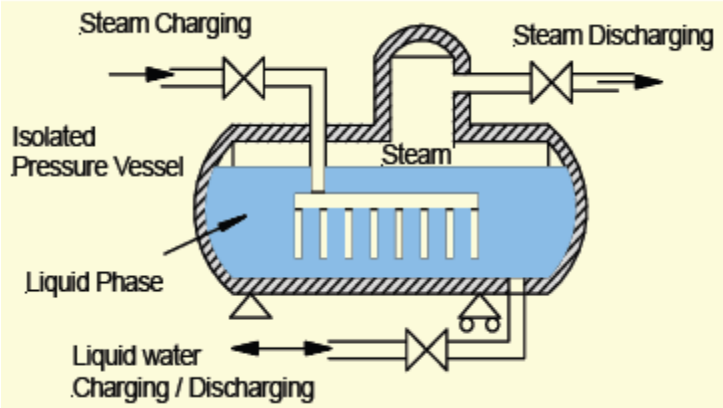

Fig. 5 - Steam accumulator scheme (Laing 2008).

- **Packed bed (and regenerators)**

  In a packed bed system the heat transfer fluid flows through a container that is full with small particles made of materials with high thermal conductivity. Regenerators are structures with high thermal conductivity and the heat transfer fluid flows through them. The regenerator concepts is a known system from the aluminum industry that is carried out at temperatures around 1100°C , usually using ceramics materials.

  This type of system is implemented in the STJ in Jülich where is used as heat transfer fluid and alumina is the storage material and its properties are shown in Table 3. The storage and heat transfer fluid are in direct contact during charging/discharging process. The air flows through small channels, this structure is typically called honeycomb brick (Zunft, Hänel et al. 2011). The system has already been tested under operating conditions between ≈200- 630°C (in March 2010) and it has a good thermal performance delivering air almost at constant temperature when discharging (Zunft, Hänel et al. 2011).

  A pebble bed regenerator was investigated by Fraunhofer UMSICHT making use of extremely small spherical materials (3 to 12 mm diameter), if alumina oxide pebbles are used the system can reach high temperatures since the maximum operating temperature for this material is 1800°C (Daschner, Binder et al. 2013).

Table 3 - Material characteristics.

Honeycombs	
Material	Alumina porcelain (C130)
Specific heat capacity	0.88 kJ/(kg·K)
Thermal conductivity	2.1 W/(m·K)

2.2.2 Latent heat storage

Latent heat storage systems make use of the release of heat during a phase change of a material. This concept has the advantage that it can occur almost at a constant temperature. The process should be reversible so the material will not change its properties after several cycles. It is also mandatory that all the material can be converted to the previous phase completely (Hasnain 1998). In this system it is even more crucial an accurate choose of material that can fit to the specific application.

2.2.2.1 Material to be used as PCM

It is expectable that the most investigated phase transition would be the transitions that release more energy, although the early investigations began with the phase change solid-liquid that usually releases less energy than the liquid-vapor transitions. This is explained that a better container is needed and also leaking problems are more likely to happen when leading with gases (Abhat 1983).

As it is mentioned above the material should match the specific operating temperature range almost perfectly. The properties of the material, even that they are similar to the properties of the materials used for sensible heat, they should have some specific performance due to their phase change usage.

The thermodynamic (A), kinetic (B), chemical (C) and economic (D) criteria used to evaluate PCM materials are (Abhat 1983):

The phase change material (PCM) should possess:

(A)

- A melting point in the desired operating temperature range;
- High specific latent heat of fusion;
- High density which reduces the container (storage) volume;
- High specific heat capacity to provide for significant additional sensible heat storage effects;
- Congruent melting: the material should melt completely so that the liquid and solid phases are identical in composition, otherwise, the difference in densities between solid and liquid cause segregation resulting in changes in the chemical composition of the material (Abhat 1983);
- Small volume changes during phase transition, so that a simple containment and heat exchanger geometry can be used (Abhat 1983).

(B)

- Little or no super cooling during freezing, the melt should crystallize at its thermodynamic freezing point. This is achieved through a high rate of nucleation and growth rate of the crystals (Abhat 1983).

(C)

- Chemical stability;
- No chemical decomposition, so that a high latent thermal energy storage system life is assured (Abhat 1983);
- Non-corrosiveness to construction materials;
- The material should be non-poisonous, non-flammable and non-explosive.

(D)

- Available in large quantities;
- Inexpensive.

In order to evaluate the properties of the material after several cycles under operating conditions, the melting and freezing characteristics of the material should be evaluated before. Abhat (1983) suggests

that two measurement techniques can evaluate these characteristics, Differential Scanning Calorimetry and thermal analysis.

Table 4 gives a summary of phase change materials. A more complete and detailed list of phase change materials is presented in Cárdenas and León (2013) work.

Table 4 - Melting temperature for different compounds

Temperature range [°C]	Material	Transition temperature [°C]	Heat of fusion [kJ/kg]
0 -100	Water Paraffin Salt hydrate	0 20-60 30-50	335 140-280 170-270
100-400	$AlCl_3$ $LiNO_3$ Na_2O_2	192 250 360	280 370 314
400-800	50LiOH/50LiF $KClO_4$ LiH	427 527 699	512 1253 2678
800-1500	LiF NaF MgF_2 Si	868 993 1271 1415	932 750 936 1654

The storage capacity of a latent heat storage system in phase transition solid-liquid is given by (4) (Portaspana 2011)

$$Q = \int_{Ti}^{Tm} m \cdot C_p \cdot dT + \cdot a_m \cdot \Delta h_m + \int_{Tm}^{Tf} m \cdot C_p \cdot dT \tag{4}$$

2.2.2.2 Latent heat storage systems

It is mentioned in the previous section that latent heat storage systems have the advantage that the process of charging and discharging can be carried out in an almost isothermal condition, making use of the heat released or consumed by phase change. Although most of the phase change materials have low thermal conductivity. In order to have an efficient latent storage system this property has been investigated recently and a lot of investigators try to find a solution to improve it (Cárdenas and León 2013).

A popular project that presented some solutions for the challenges in latent heat storage systems is the DISTOR project (Steinmann and Tamme 2008). The solutions presented in the project are:

- **Extended heat transfer area**

  This approach suggests that if the heat transfer fluid's container area in contact with the PCM is larger the phase change will occur faster because the distance for heat transfer between the container and the solid PCM is reduced.

- **Composite material with increased thermal conductivity**

  Materials with extremely high thermal conductivity are added to the PCM.

Some applications using these solutions are presented on the following section.

2.2.2.3 Examples of latent heat storage systems

- **Sandwich design**

  Typically, latent heat storage systems consist of a tube (or container) where the heat transfer fluid is flowing and this tube is in contact with the phase change material. When charging, usually the phase change material is changing its phase from solid to liquid. If the thermal conductivity of the phase change material is low, the process is much slower and inefficient and what can occur is that part of the material is still solid by the end of the charging period.

  The sandwich design consists in the addition of a structure, in between of the phase change material, with high thermal conductivity. These structures are added in parallel to to each other and perpendicular to the tube containing the heat transfer fluid (Steinmann and Tamme 2008).

  Fig. 6 shows the scheme of a storage unit of the sandwich concept. Foils made of exfoliated graphite are combined with PCM to form a sandwich structure.

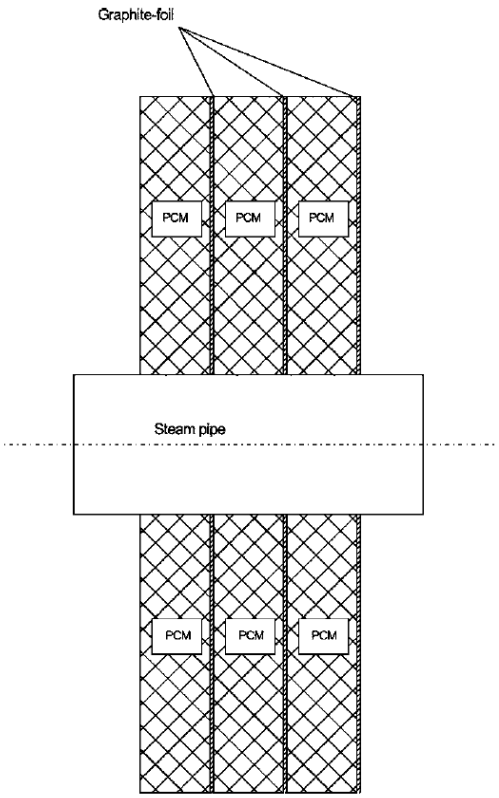

Fig. 6- Schematic of the sandwich concept using graphite foil (Steinmann and Tamme 2008).

- **Cascaded PCMs**

  The latent heat storage systems, as it is mentioned before, make use of a phase change in a material that occurs almost at constant temperature. The performance of these systems depends on the temperature difference between the PCM and the heat transfer fluid. During charging process the heat transfer fluid is transferring heat to the PCM that is changing its phase, although the heat transfer fluid will also decrease its own temperature. Which means that until the heat transfer fluid leaves the system on the outlet the process is less efficient on the end part of the system (if we only consider along the x axis).

  Some investigations suggest that if the difference between the PCM and the heat transfer fluid is kept constant along the whole process the system has a much better performance. What the

investigations suggest is that a series of PCM is placed in series next to each other, where the phase change temperature is lowering from the left (inlet during charging) to the right (outlet during charging) this temperature is constant along the whole process and a constant heat flux is also achieved, this approach is usually called cascaded PCM (Jegadheeswaran and Pohekar 2009). Fig. 7 shows an example of a cascaded heat storage system.

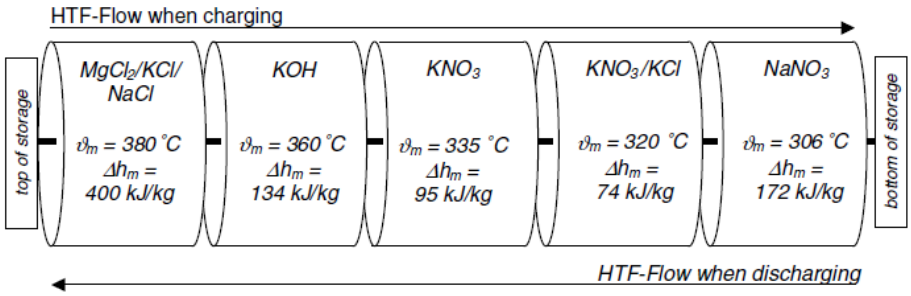

Fig. 7 - Example of a cascaded latent heat storage system (Michels and Pitz-Paal 2007).

Experimental investigations with three PCMs, sodium nitrate $NANO_3$ a eutectic mixture of potassium nitrate and potassium chloride KNO_3/KCl and potassium nitrate KNO_3, were carried out by (Michels and Pitz-Paal 2007) .

Michels and Pitz-Paal (2007) work show that when this approach is used a bigger amount of PCM changes its phase when compared with systems that only use a single PCM, they determined that when using the cascaded approach the PCM material that experiments a phase change is around 92% during charging process and 67% during discharging process. Even when using a single PCM that the whole material experiences a phase change during charging process, during discharging process only 2% of the material experiences a phase change.

- **<u>Lithium carbonate Li_2CO_3 prototype</u>**

  This prototype uses Lithium carbonate Li_2CO_3 as PCM material and makes uses of copper to improve the thermal performance of the PCM. Verdier, Ferrière et al. (2014) performed numerical simulations that can be analyzed. The system is in equilibrium, ate the beginning, and is set on a uniform temperature of 700°C. To charge the system, a temperature of 900°C is set as boundary condition on the bottom part of the structure. To evaluate the discharging process of the system a boundary condition of 100°C is set on the bottom of the structure, and before the discharging process begins, a uniform temperature of 900°C is assumed for the system. The concept of the system analyzed is showed in Fig. 8.

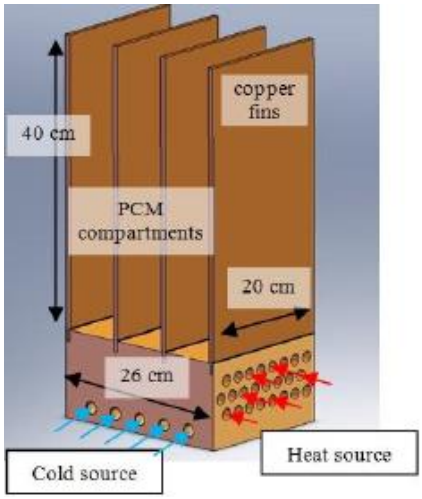

Fig. 8 - 3D representation of the concept (Verdier, Ferrière et al. 2014).

The numerical results are shown in Fig. 9.

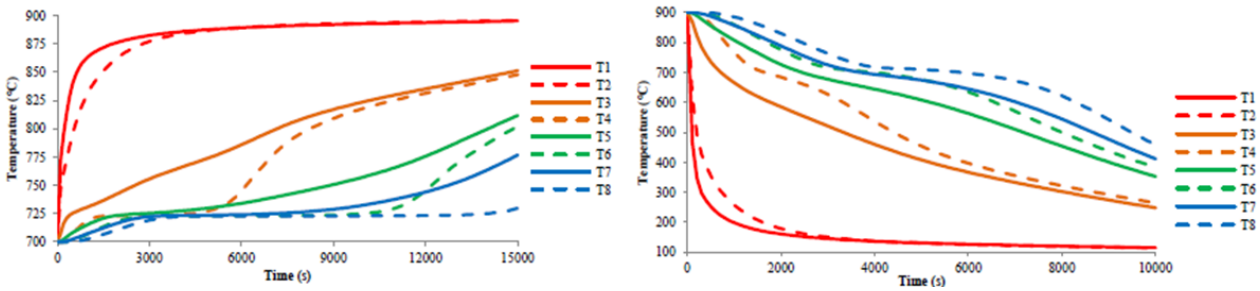

Fig. 9 - Evolution of the PCM temperature during heating (left) and cooling (right) phase (Verdier, Ferrière et al. 2014).

T1, T3, T5, and T7 are temperatures closer to the fin and T2, T3, T4, and T8 are located in the center of the compartment.

Fig. 9 shows the results of the numerical investigations performed by Verdier, Ferrière et al. (2014). Here a comparison with a system using only PCM without the copper fins was not made. So the only results that can be evaluated is that the system takes around 4h to be completely charged and 2.5h to be completely discharged.

More investigations and comparisons between traditional latent heat storage systems and system with the integration of material with high thermal conductivity should be made to really determine its advantages and influences on the system.

2.2.3 Thermochemical heat storage

On thermochemical heat storage it is taken advantage of enthalpy but instead of a phase change, like in latent heat storage, this system makes use of the completely reversible endothermic chemical reactions. The concept of this system is to absorb the excess heat in an endothermic reaction and store the products on separate containers. During discharging the products are combined exothermically and the heat of reaction can be used.

These systems are far behind in maturity when compared with sensible or latent heat storage systems but they represent a promising solution due to their high energy density and by the possibility to store energy at ambient temperature.

Like the other systems presented above a proper choice of the materials should be evaluated, on the next section the material choice and properties are presented.

2.2.3.1 Properties of reactions considered for thermochemical energy storage systems

On thermochemical the properties are related to compounds and reactions. On this type of storage systems the properties chased are even more peculiar and crucial.

Necessary properties of the compounds, to be used as thermochemical heat storage, as told in Portaspana (2011) work, are:

- **Reversibility**

  No side reactions or changes in reaction rate with the time should occur. The reaction should be completely reversible (Portaspana 2011).

- **Reaction rates**

  Both forward and reverse reactions must be rapid enough to absorb all the available energy or release it promptly. The reaction rates must not decrease with cycling. Such a decrease can be observed, if structural changes of the storage medium occur (Portaspana 2011).

- **Controllability**

  The reactions must be controllable because they have to be turned on and off when required. Controllability is achieved by product separation, by controlling the temperature and pressure, or by catalysts (Portaspana 2011).

- **Ease of storage**

  The reaction products have to be easily separable prior to storage. Reactions must not occur at storage temperature (Portaspana 2011).

- **Safety**

  Toxicity, inflammability, and corrosiveness of the reaction products may pose unacceptable safety hazards (Portaspana 2011).

- **Cost**

  Cost should be as low as possible which requires materials which are readily available (Portaspana 2011).

On the following section will be presented some reactions considered for thermochemical heat storage.

2.2.3.2 Examples

- **Ammonia dissociation**

  When a thermochemical heat storage system is being implemented it will occur in a reactor. An important detail when evaluating promising reactions is if the process is already well-known in other applications. This is the case of ammonia dissociation reaction (5), the heat recovering reaction is the well-known Haber Bosch process, usually employed for fertilizer production. Ammonia dissociation has other advantages such as no side reactions occur and it consists of no aggressive reactants for the environment. On the other hand ammonia dissociation has a relatively low enthalpy of reaction around 66.5 kJ/mol (Lovegrove, Luzzi et al. 1999). Most of the studies on this reaction as a heat storage system have been carried out by the Australian National University.

$$NH_3 + \Delta H \Leftrightarrow \frac{1}{2} N_2 + \frac{3}{2} H_2 \tag{5}$$

- **Reduction and oxidation reactions**

  This is a two-step concept that makes use of the principle of transition between the oxidized and reduced form of an oxide of a metal that has multiple oxidation states (Agrafiotis, Roeb et al. 2014).

  On the first step an endothermic reaction (6) takes place, with the supply of external heat the reduced state of the oxide MeO_{ox} is obtained as a product (Agrafiotis, Roeb et al. 2014). The general reaction is:

$$MeO_{ox} + (\Delta H) \Leftrightarrow MeO_{red} + O_2(g) \tag{6}$$

  On the second step an exothermic reaction (7) takes place via an oxygen source. If air is used as the oxygen source the oxidation reaction is as the same structure as (Agrafiotis, Roeb et al. 2014):

$$MeO_{red} + O_2(g) \Leftrightarrow MeO_{ox} + (\Delta H) \quad (7)$$

Agrafiotis, Roeb et al. (2014) present the relevant reversible reactions considered for thermochemical processes as scheme (8) for metal hydroxides, scheme (9) for carbonates and scheme (10) for oxides.

$$Ca(OH)_2 + (\Delta H) \Leftrightarrow CaO + H_2O \qquad \Delta H = 100 kJ/mol_{react} \quad (8)$$

$$CaCO_3 + (\Delta H) \Leftrightarrow CaO + CO_2 \qquad \Delta H = 167 kJ/mol_{reac} \quad (9)$$

$$Co_3O_4 + (\Delta H) \Leftrightarrow 3CoO + \frac{1}{2}O_2 \qquad \Delta H = 200 kJ/mol_{reac} \quad (10)$$

Heating cycles between 985 and 785°C were performed by Tescari, Agrafiotis et al. (2014) in Co_3O_4 as well as Co_3O_4 – based binary powder metal oxide compositions under air. They showed on their work that the reactions are completely reversible. Tescari, Agrafiotis et al. (2014) investigated an hybrid system. This hybrid system consists of coating a typical honeycomb sensible heat storage system. The investigation suggests that the system will have a similar behavior to the plain powder thermochemical system and will improve the ceramic honeycomb system by increasing the amount of energy stored by the system

Cobalt oxide powder was compressed and become a cobalt oxide pellet and was tested by Karagiannakis, Pagkoura et al. (2014). Their work shows that the pellet can slightly improve the performance of the chemical reaction. The results for powder and pellet can be seen in Fig. 10.

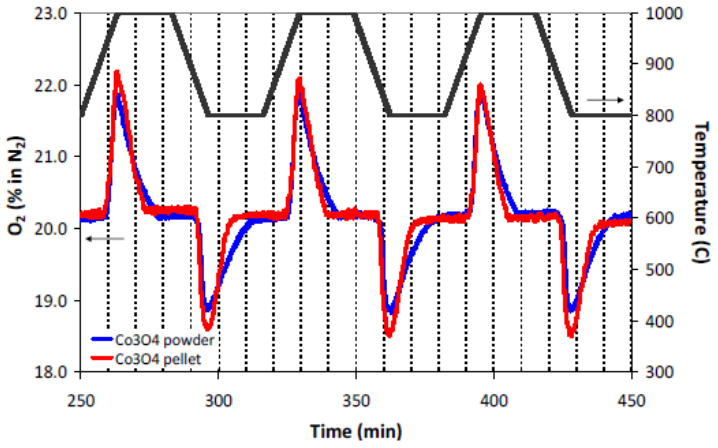

Fig. 10 - Comparison of thermochemical redox behavior of cobalt oxide in powder and pellet form (Karagiannakis, Pagkoura et al. 2014).

In Fig. 10 the red line represents the cobalt oxide pellet and the blue line represents the powder. And by analyzing the peaks it is possible to understand that it is possible to operate in a wider range of temperatures and recover more heat from the reaction.

Miguel, Gonzalez-Aguilar et al. (2014) are on the early investigations for a fluidized bed system considering the manganese (III) redox reaction showed in (11).

$$6Mn_2O_3 \Leftrightarrow 4Mn_3O_4 + O_2 \qquad \Delta H = 31.8 kJ/mol \text{ of } Mn_2O_3 \quad (11)$$

- **<u>Sulfur based thermal energy storage</u>**

This thermochemical storage concept consists on storing energy by producing elemental sulfur for later burning. To produce elemental sulfur on a thermochemical process three chemical reactions take place: (12) concentrated sulfuric acid is decomposed by heat into water, sulfur dioxide, and oxygen; (13) sulfur dioxide undergoes disproportionation in water into sulfuric

acid and elemental sulfur; (14) the sulfur generated is directed to storage and/or to a sulfur burner for combustion to generate heat. The thermochemical cycle does not produce waste effluent and does not emit greenhouse gas into the environment (Bunsen Wong 2013).

$$H_2SO_4 \text{ Decomp.}: 2H_2SO_4(l) \rightarrow 2H_2O(g) + O_2(g) + 2SO_2(g) \qquad \Delta H \approx 97 kJ/mol \tag{12}$$

$$SO_2 \text{ Disproportion}: 2H_2O(l) + 3SO_2(g) \rightarrow 2H_2SO_4(aq) + S(s,l) \tag{13}$$

$$S \text{ Combustion}: S(s,l) + O_2(g) \rightarrow SO_2(g) \qquad \Delta H = -297 kJ/mol \tag{14}$$

3. Mathematical model

3.1 Introduction

In this chapter, the thermal interaction between the heat transfer fluid and the storage material of the system is studied mathematically.

The system studied is similar to the one installed in the STJ (Zunft, Hänel et al. 2011), using air as heat transfer fluid and alumina as storage material.

The model objective is to simulate a dynamic state of the thermal storage system during charge and discharge process as well as to switch between these processes in a continuous simulation run. This ability of switching between charging and discharging conditions in one simulation is of crucial importance in order to enable the complete simulation of the solar methane reforming plant where the model will be integrated. Determining the relation between the total volume of the storage system and the number of hours that it can provide heat to operate the plant is also a goal of this work.

The model discretizes the storage in a large number of interacting layers providing detailed information about the temperature distribution within the storage. Air flows through the honeycomb bricks channels to transport the heat to or from the storage. The convective heat transfer coefficient between air and solid is sufficiently large which leads to a small temperature difference between air and solid during charging or discharging of the system.

The storage model presented in this work assumes an ideal storage, which means that no heat losses are taken into account during charging or discharging period. During standstill period (when air is not flowing through the channels) the temperature gradient will remain the same until the next charging or discharging period starts again.

The temperature dependent properties of air and the pressure loss by forced convection have been considered in this model.

The storage model is implemented in Aspen Custom Modeler® with the appropriate syntax shown in Appendix A - Aspen Custom Modeler, Model Code.

In order to reduce the computations time only a single channel of one honeycomb brick is simulated. The same conditions are assumed for each parallel channel so that all the channels will have a similar behavior since no heat losses to environment are considered. The energy stored by the system is then the product of number of channels by the energy stored in only one channel.

3.1.1 Storage structure

As mentioned in the previous sections the system modeled is similar to the system installed in STJ. The system installed in STJ consists of a storage chamber made of honeycomb storage elements as shown in Fig. 11.

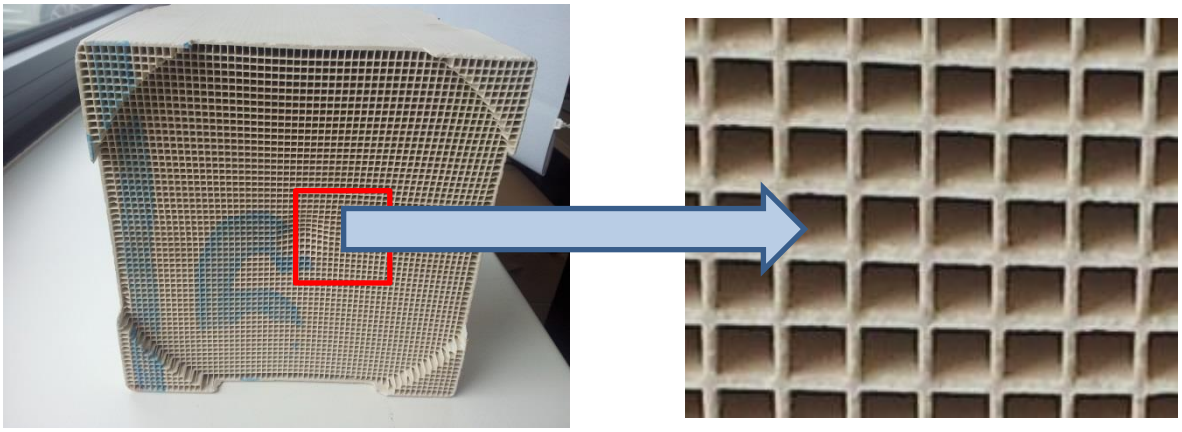

Fig. 11 - Honeycomb brick.

The model will only consider the volume of material capable of storing energy, which is the volume of honeycomb bricks, excluding the housing and insulation material. The model does not consider any degradation after a long operating period.

3.1.1 Storage system general properties

The storage installed in STJ is a regenerator-type. Air flows from the top to the bottom of the system in direct contact with the alumina structure during charging period. During discharging the air flow is reversed.

The system installed in STJ is a block with a volume of 120m^3 and a height of 3m and operates between 680 and 120°C with a nominal charge mass flow of 9.4 kg/s. Table 5 is a summary of the storage specifications (Zunft, Hänel et al. 2011).

Table 5 - Storage specifications.

Storage specifications	
Temperature range	680 – 120 °C
Charge mass flow	9.4 kg/s
Pressure loss	<1500 Pa

The storage material used is alumina porcelain (C130) and its thermophysical properties are shown in Table 6 (Zunft, Hänel et al. 2011).

Table 6-Alumina porcelain (C130) properties.

Honeycombs	**60 x 60 channels**
Brick dimensions	15 x 15 x 15 cm
Mass density	2700 kg.m-3
Specific heat capacity	0.88kJ.(kg-1.K-1)
Themal conductivity	2.1 W.(m-1.K-1)
Heating surface 1180	m2.m-3

3.1.1 Honeycomb storage principle

The principle of the honeycomb ceramic is identical to other sensible heat storage. During the charging period the hot air flows through the systems micro-channels and releases heat, increasing the material temperature. During the discharging period the flow direction is reversed and then cold air flows through the systems micro channels and absorbs the heat stored in the material, resulting in an increase of the air temperature.

As Luo, Wang et al. (2013) showed the honeycomb ceramic have an excellent heat transfer characteristic resulting from the larger heat exchange area and fine flow behavior, meaning relatively small pressure drop resulting from the flow-through channels.

3.2 Physical model

Fig. 12 shows the physical model which consists of a quadrangular channel with length L and opening s. During the charging process, heated air flows through the channel from top to bottom of the channel. During the discharging process the air flow is reversed and cold air is pumped from the bottom to the top of the channel.

The channel is discretized in a certain amount of points, between 0 and L, with the same spacing between each other. The spacing between each point will return more or less accurate results for a smaller and larger spacing, respectively. The spacing will also influence the simulation time so a optimal situation should be determined, where a not so time consuming simulation can be carried out with reasonable accurate results.

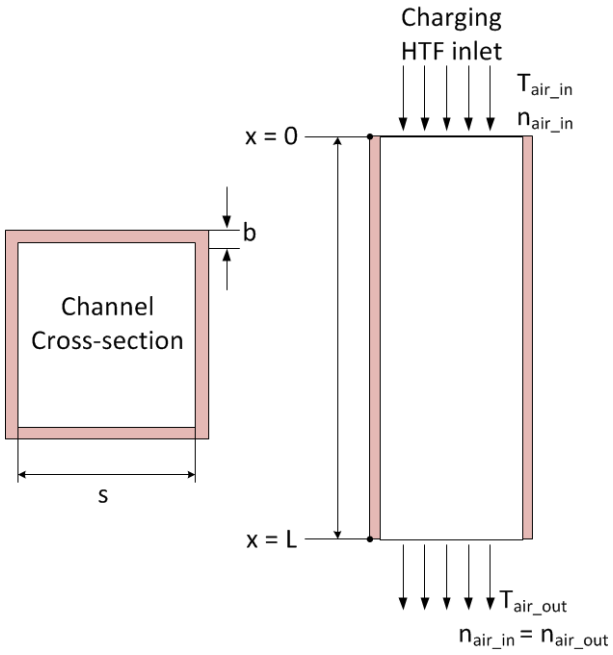

Fig. 12 - Physical model of the storage system.

A temperature gradient is achieved during both processes and the system is considered completely charged when the air temperature in the outlet exceeds the defined minimum temperature, that should usually be defined according to the outlet temperature of the process, i.e. heat exchangers, that the heat is used in. In opposite, the system is considered completely discharged when the air outlet temperature during discharge decreases below the required higher temperature level. A representative scheme of the thermal gradient in the system is shown in Fig. 13.

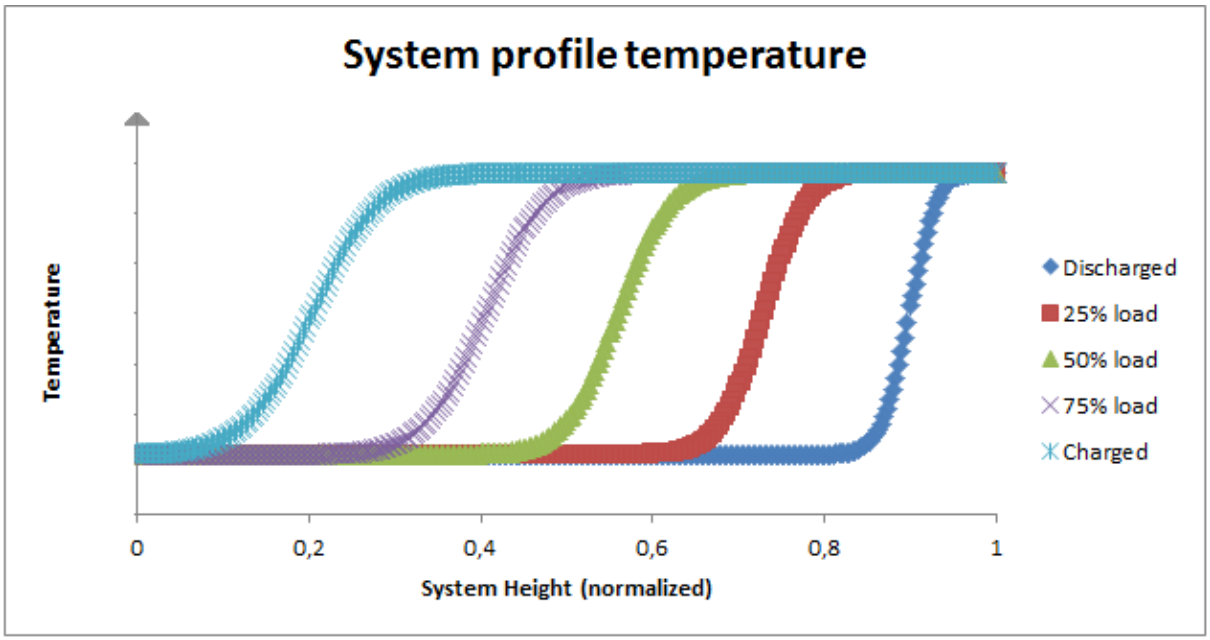

Fig. 13 - Representative thermal gradient in the storage system.

3.3 Governing Equations

The storage system modeled is a regenerator-type heat storage. A regenerator is a type of heat exchanger in which the hot and cold-fluids occupy the same physical space, but at different times. Regenerators necessarily operate in a transient mode. The temperatures throughout the system depend upon time as well as on position. Partial differential equations are needed to describe the time and spatial dependence of the temperature of the solid and the fluid. These equations can be identified using energy balances on the fluid and solid (Nellis and Klein).

The energy equations used to describe the model follow the descriptions and assumptions listed below:

- Ideal behavior of the system, the amount of energy recovered is the same as the amount stored.
- The fluid flow inside the storage is vertical, from top to bottom during charging and from bottom to top during discharging.
- The fluid thermophysical properties are temperature and pressure dependent.
- The solid thermophysical are temperature independent.
- There is no heat generation or dissipation inside the storage.
- The system is well insulated and there are no losses to the ambient.
- Pressure drop along the channel is considered.
- The system is one dimensional, only temperature gradients along the x axis.

The energy equation for the fluid (15) is written as

$$n_{air} \cdot c_{p,air} \cdot \left(\frac{\partial T_{air}}{\partial x}\right) + \rho_{air} \cdot c_{p,air} \cdot A_{cs,air} \cdot \left(\frac{\partial T_{air}}{\partial t}\right) = 4 \cdot \alpha \cdot s \cdot (T_{air} - T_{sol}) \quad (15)$$

The first term on the left side of the equation corresponds to the enthalpy associated with the fluid flow. The second term on the left side of the equation corresponds to the rate of change of enthalpy. The term on the right side of the equation corresponds to the heat exchange by convection between the solid and the fluid. The conduction in the fluid can be neglected due to the small value of air conductivity.

The energy equation for the solid (16) is written as

$$\rho_{sol} \cdot c_{p,sol} \cdot A_{cs,sol} \cdot \left(\frac{\partial T_{sol}}{\partial t}\right) = A_{cs,sol} \cdot k_{sol} \cdot \left(\frac{\partial^2 T_{sol}}{\partial x^2}\right) + 4 \cdot \alpha \cdot s \cdot (T_{air} - T_{sol}) \quad (16)$$

The term on the left side of the equation corresponds to the change of enthalpy of the solid. The first term on the right side of the equation corresponds to the heat transferred by conduction in the solid along the x axis. The second term on the right side corresponds to the heat transferred by convection between the particles and the fluid.

It is necessary to evaluate the convective heat transfer coefficient, α, to determine the heat transferred by convection. The convective heat transfer coefficient is affected by the state of the flow and the shape of the duct and can be determined by (17) using the appropriate *Nusselt* correlation. The heat transfer convective coefficient is determined locally by the model.

$$\alpha = \frac{Nu \cdot \lambda_{air}}{s} \quad (17)$$

In order to use the appropriate correlations an evaluation of the flow state is needed, this evaluation is determined by the Reynolds number. A flow is laminar if Re ≤ 2400 and turbulent if Re ≥ 4000, in between, the flow is in a phase called transition (Yunus and Cimbala 2006). In the presented model the Reynolds number range is from ≈7 – 12, meaning that the flow is in laminar phase. The appropriate *Nusselt* correlation is a correlation that gives the *Nusselt* number for a fully developed laminar flow transferring heat to four walls in a quadrangular duct (18) (Shah and London 1978) which depends on the side length of the duct entry cross section.

$$Nu = 8.235\,[1 - 2.0421 \cdot a + 3.0853 \cdot a^2 - 2.4765 \cdot a^3 + 1.0578 \cdot a^4 - 0.1861 \cdot a^5] \quad (18)$$

with $a = \frac{c}{d}$

$\underline{a}$ represents the relation between the side length of the duct entry cross section and it is equal to one for quadrangular ducts.

3.3.1 Boundary and initial conditions

The temperature in the fluid and solid can be determined by (15) and (16), respectively. The solution of the temperatures depends on the physical conditions existing at the boundaries of the system. An initial condition is also needed since the system is also time dependent.

The boundary condition to solve the fluid equation (15) is:

- The air inlet temperature is constant for all time

$$T(0,t) = T_{air,in} \quad (19)$$

The boundary conditions to solve the solid equation (16) are:

- In the first layer of the solid (since there is no previous layer) the conduction is only to the next layer so the second derivative term becomes a first order derivative term

$$\rho_{sol} \cdot c_{p,sol} \cdot A_{cs,sol} \cdot \left(\frac{\partial T_{sol}}{\partial t}\right) = A_{cs,sol} \cdot k_{sol} \cdot \left(\frac{\partial T_{sol}}{\partial x}\right) + 4 \cdot \alpha \cdot s \cdot (T_{air} - T_{sol}) \quad (20)$$

- In last layer of the solid (since there is no next layer) the conduction is only form the previous layer so the second derivative term becomes a first order derivative term

$$\rho_{sol} \cdot c_{p,sol} \cdot A_{cs,sol} \cdot \left(\frac{\partial T_{sol}}{\partial t}\right) = A_{cs,sol} \cdot k_{sol} \cdot \left(\frac{\partial T_{sol}}{\partial x}\right) + 4 \cdot \alpha \cdot s \cdot (T_{air} - T_{sol}) \quad (21)$$

- The initial conditions at the beginning of the simulation are defined by the solid temperature. The system is in equilibrium and the fluid temperature inside the channel is equal to the solid temperature

$$T_{air}(x,0) = T_{sol}(x,0) \tag{22}$$

3.3.1 Pressure drop

Pressure drop is a quantity of interest since it is directly related to the power requirements of the fan or pump to maintain flow, which will be further considered when the model is implemented in the solar methane reforming plant model.

The pressure drop inside the channel is considered and was determined by (23) from Yunus and Cimbala (2006).

$$\Delta p = f \cdot \frac{L}{D} \cdot \frac{\rho_{air} \cdot V_{air}^2}{2} + \rho_{air} \cdot g \cdot L \tag{23}$$

f is the Darcy friction factor and it is defined as (24) for fully developed laminar flow in a quadrangular duct.

$$f = \frac{56{,}92}{Re} \quad , \quad Re = \frac{VD}{\nu} \; and \; Re \leq 2300 \tag{24}$$

3.3.1 Energy balance

In order to make sure that the energy gain by the wall during charging process or the energy loss by the wall during discharging process, is the same as the air enthalpy change and make sure that the model does not violate the first principle of thermodynamics (conservation of energy), two monitoring variables were created and their values compared.

These two variables are the solid enthalpy change, determined by (25) and the air enthalpy change (26).

$$Q_{st,wall} = \rho_{sol} \cdot c_{p,sol} \cdot A_{cs,sol} \cdot L \cdot \left(\frac{\partial T_{sol}}{\partial t}\right) \tag{25}$$

$$Q_{air} = n_{air} \cdot [h_{air}(L) - h_{air}\,(0)] \tag{26}$$

3.4 Model Validation

Is necessary to check the model performance with already existing validated models or compare the model with experimental data. In order to compare the model with experimental data it is necessary to recreate the model as much close to the real system.

To validate this model, experimental data and previous works from the system installed in STJ are available (Zunft, Hänel et al. 2011, Kronhardt, Alexopoulos et al. 2014). To validate the model the same properties from the system installed in the STJ are implemented in the model.

A comparison between the model implemented in Aspen Custom Modeler and a model built in Comsol Multiphysics® will also be shown in this chapter.

3.4.1 Comparison with experimental data

A test campaign was performed by Zunft, Hänel et al. (2011) in March 2011. These experiments had the goal to evaluate the storage performance and the validation of existing simulations and design tools.

The experiments include charging period, standstill and discharging performance of the storage system. Different inlet air temperatures and different inlet mass flows were tested and measured in the test campaign. The experimental data is not published in detail.

The measured data was difficult to interpret and due to lack of information regarding the thermocouples location it was not possible to achieve the correct interpretation of the measured data and it was not also possible to establish a comparison between the model presented in this work and the test campaign performed by Zunft, Hänel et al. (2011).

3.4.1 Comparison with previous validated models

The model presented by Hirsch, IRT et al. (2012) was validated using measured data from the system installed in STJ. The test boundaries as mass flow, inlet temperature and inlet pressure, are the nominal solar tower process values showed in Table 5. The initial temperature gradient inside the system presented by Hirsch, IRT et al. (2012) was determined by interpolation of the real temperature of the storage (this initial gradient is not the discharged gradient, it is just the reference point before one hour charging period). Under these conditions this model is appropriate for validation of the model created in this work.

The comparison between the initial gradient in our model and the model by Hirsch, IRT et al. (2012) is shown in Fig. 14. The results show a good agreement.

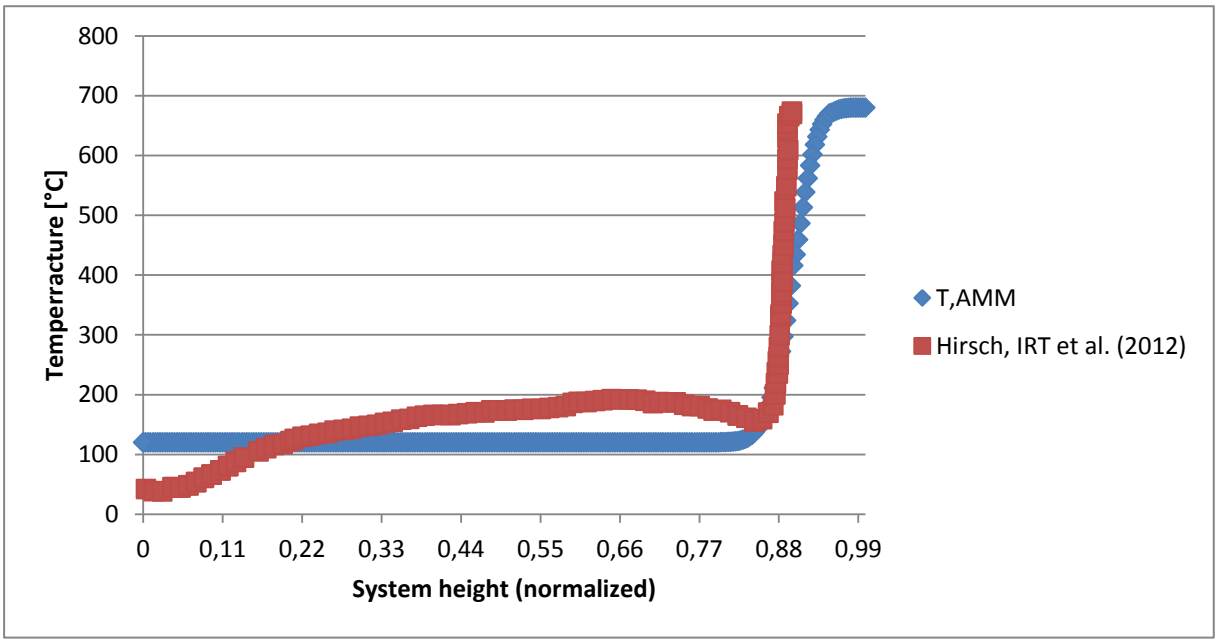

Fig. 14-Initial gradient comparison between aspen model and (Hirsch, IRT et al. 2012) model. Horizontal axis is normalized.

Another comparison is shown in Fig. 15, this comparison is the systems profile temperature after one hour charging. Once again the presented model and the model presented by Hirsch, IRT et al. (2012) show a good agreement. The deviations can be due that in our model a constant inlet mass flow and inlet temperature is assumed for the whole hour leading to no oscillations. Also the difference in the initial gradient leads to higher deviations between the two models. It is expected that when the system reaches a periodic steady state operating conditions the deviations are reduced.

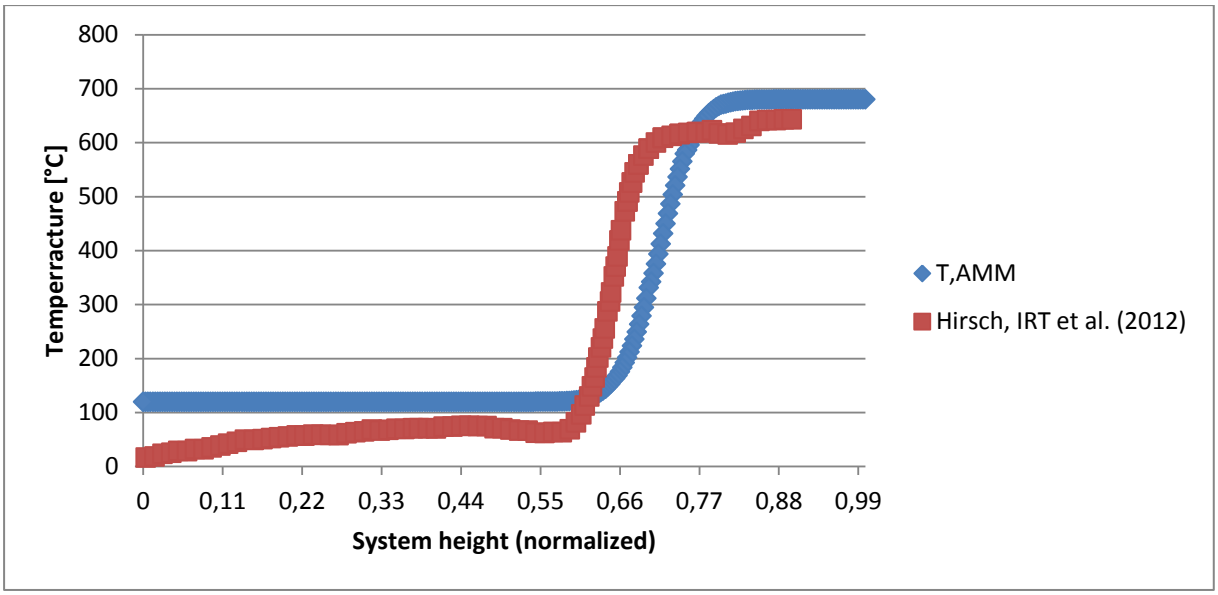

Fig. 15 - After one hour charging gradient comparison between Aspen model and (Hirsch, IRT et al. 2012) model. Horizontal axis is normalized.

3.4.1 Comparison with a Comsol Multiphysics® model

The model presented in this work simulates the behavior of one channel of the whole system. A channel of the whole system is a certain number or honeycomb bricks disposed in series on top of each other until it reaches 3 meter high. In our model to achieve the 3 meter height 20 models are connected in series, since every honeycomb brick has 15cm length as shown in Table 6.

Aspen Custom Modeler® is a powerful tool and enables to perform complex calculations and simulations using a simple syntax and in short period of time. Comsol Multiphysics® model is also a powerful tool and also enables the creation of a 3D picture of the system. In order to get a better understanding of the system a simple Comsol Multiphysics® model was created.

- ***Comsol Multiphysics® model***

  The comsol model consists of a honeycomb channel. The alumina properties applied are the same shown in Table 6 and the air themophysical properties are temperature dependent.

  The boundary conditions applied in the *Comsol* model are:

  - Constant inlet temperature of 680ºC
  - Adiabatic outer walls of the channel
  - Constant inlet pressure
  - Outlet velocity ≈0.06 m/s

The system is in an equilibrium state of 150ºC in the beginning. The system is evaluated after one hour under these conditions and results are presented in Fig. 16.

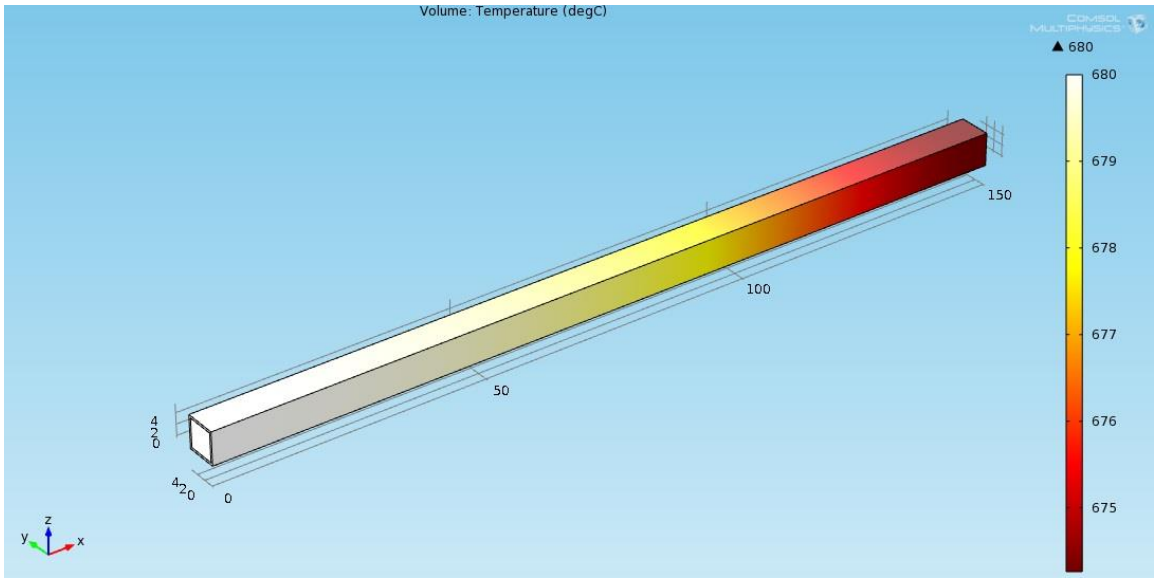

Fig. 16 - Comsol results after one hour simulation.

When this model is compared with the model created in Aspen that need to be connected in series the results shown a good agreement with slight deviations. The results curves are shown in Fig. 17. In Fig. 17, T,comsol corresponds to the *Comsol* model data, T,AMM corresponds to the model created in Aspen where several models are connected in series and T,ALCM corresponds to the model created in aspen where a single long channel is simulated.

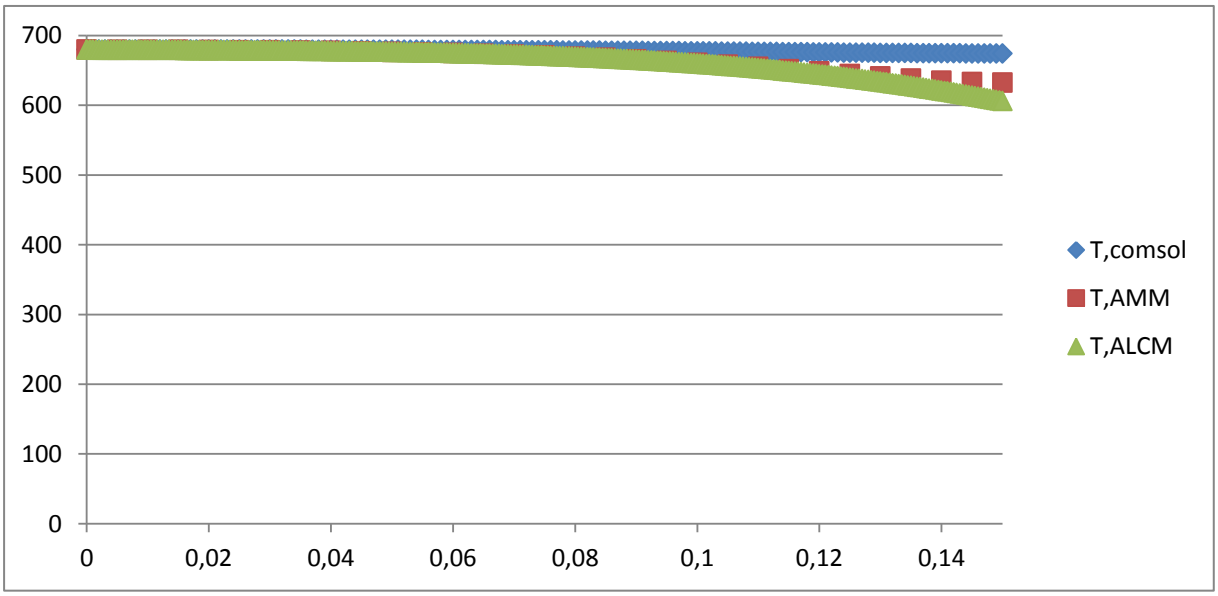

Fig. 17 - Comparison with comsol model.

3.4.1 Comparison between Aspen Models

The model presented in this work shows a good agreement with validated models using measured data. But in order to implement our model in the complete solar methane reforming process model this connection of blocks is extremely difficult to handle when a transient simulation is carried out due to the fact that the charging outlet becomes the inlet during discharging of the system. In order to simplify this issue a single model of 3 meter height was created. The main difference between a model of 3m length and 20 models of 15cm length connected in series is that in the 3m length single model, thermal conduction between 2 consecutive bricks occurs.

In order to make sure that thermal conduction between consecutive bricks will not lead to inaccurate results the two aspen models are compared. The curve of the first 15cm of the long channel aspen model (represents the first brick) is also plotted in Fig. 17. In the end of the curve a slight deviation from the *Comsol* model and the aspen multiple bricks model can be noticed.

Although, if the complete systems are compared they show a good agreement, here for simplification a *Comsol* model is not considered.

Regarding the conduction in a long channel can lead to high deviations in low dimensions, as shown in Fig. 17, but when compared to the complete system these deviations are negligible as shown in Fig. 18 where the series connected model and the single long model in Aspen are compared. In Fig. 18 the curves cannot even be distinguished due to superposition.

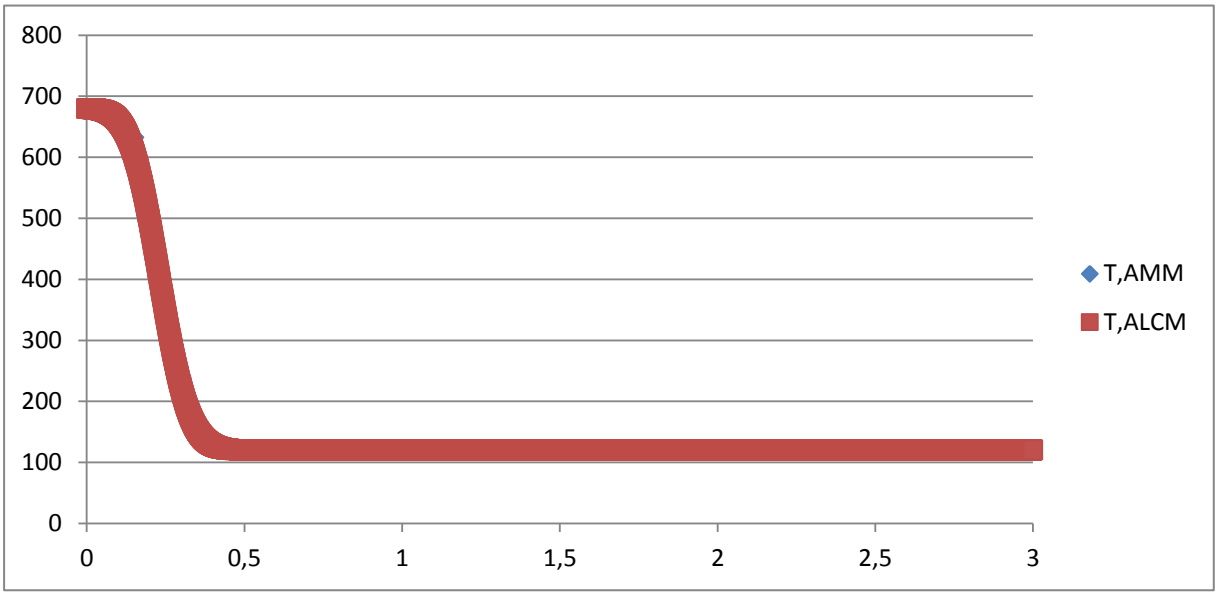

Fig. 18 - Comparison between the two different Aspen models.

3.5 Validation discussion

The model created is validated with the previous shown data comparison. In order to reduce the simulation time and the complexity of the system, a model of a long single brick will be used to simulate the system in operation and implemented in the complete solar methane reforming process model. Although, this assumption is not completely accurate, the deviation from accurate modelling is small as the validation shows.

In the next section a sizing of the system to be implemented will be shown since the solar methane reforming plant characteristics are different from the STJ.

4. System sizing

4.1 Introduction

In this section, a relation between the total volume of the storage material and the solar methane reforming plant operating hours is presented.

As shown in Fig. 19, the air is heated up in the solar receiver and pumped to the reformer. The solar methane reforming is designed to operate under constant conditions, which means that the air mass flow and temperature reaching the reformer should be constant during operation. The heat storage system is implemented in parallel to the reformer, and the exceeding air during solar radiation period is used to charge the heat storage system.

The charging mass flow to the heat storage system is adjusted, enabling a constant air mass flow delivered to the reformer, at a constant temperature of 900 °C.

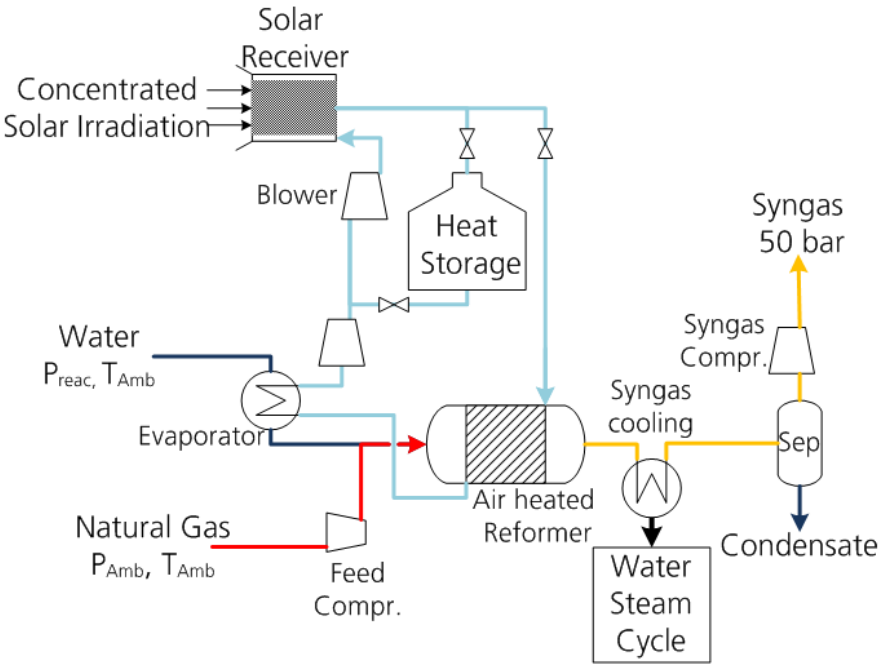

Fig. 19 - Solar methane reforming plant with storage scheme.

4.2 Mass flow variation

The air mass flow available at 900 °C depends on the incident solar radiation at a certain time. If the intercept radiation is lower than 15 MWh no air mass flow is available at the desired temperature and 52.5 MWh is the maximum intercept radiation available.

The air mass flow available to the storage system can be determined by (27). The total air mass flow available varies with the time due to the solar radiation and the air mass flow to the reforming process is constant.

$$\dot{n}_{air\ to\ storage} = \dot{n}_{air\ total} - \dot{n}_{air\ to\ reformer} \tag{27}$$

Data for the intercept radiation for each hour of the year and the respective air mass flow available for one channel of the system is evaluated and the first 58 hours correspondences are shown in Appendix B.

4.3 Energy available

The energy available for storage will be the enthalpy variation of the correspondent air mass flow available for the storage system during that hour.

The outlet temperature of the air after the reforming process is 368 °C, and this also corresponds to the outlet temperature of the heat storage system during charging period. The energy available will be the enthalpy variation of the air from 900 to 368 °C and it is determined by (28).

$$\dot{Q}_{to,storage} = \dot{n}_{air\ to\ storage} \cdot [h_{air,900} - h_{air,368}] \tag{28}$$

A balance for each hour of the year is done (29). During charging period the energy stored is summed and subtracted if a discharging period is taking place. With this energy approach a maximum energy stored in the system is determined.

$$Q_{Storage}(t + \Delta t) = Q_{Storage}(t) + \dot{Q}_{to,storage} \cdot \Delta t \tag{29}$$

4.4 Operating hours

The operating hours will vary with the air mass flow designing point of the solar methane reforming plant.

If the air mass flow is set to a low value, a higher air mass flow is available to store energy in the storage system. This will enable the solar methane reforming to operate for more hours and the plant size decreases for a fixed product output when the operating hours are increased. In an extreme scenario the solar methane reforming plant could operate the 8760 hours of one year. Although that the plant could operate the whole year this is not the optimum scenario since the storage volume required would become huge.

4.5 System volume and shape

The volume of the storage material needed will vary with the operating hours. A bigger volume is needed for more operating hours and a smaller volume is needed for less operating hours.

The shape will affect mainly the pressure drop of the system, which increases with the length of the system.

Knowing the maximum energy to be stored in the system (determined on the previous point), the material mass density, the material heat capacity and the temperature difference that the system will operate (in the solar methane reforming plant the temperature range is 900 – 368 °C) the storage material volume needed can be determined by (30).

$$V_{storage} = \frac{Q_{to,storage,max}}{\rho_{sol} \cdot c_{p,sol} \cdot \Delta T} \tag{30}$$

4.6 System design

With all the information presented in the previous points it is possible to establish a relation between the operating hours of the solar methane reforming plant and the volume of the storage material. This relation is shown in Fig. 20. The maximum of the storage material needed is reached if the plant is operated continuously for the whole year. But this relation is not linear and if the plant is operated for around 80% of the time the storage material volume needed decreases to around 5% of the maximum volume needed to operate 100% of the time.

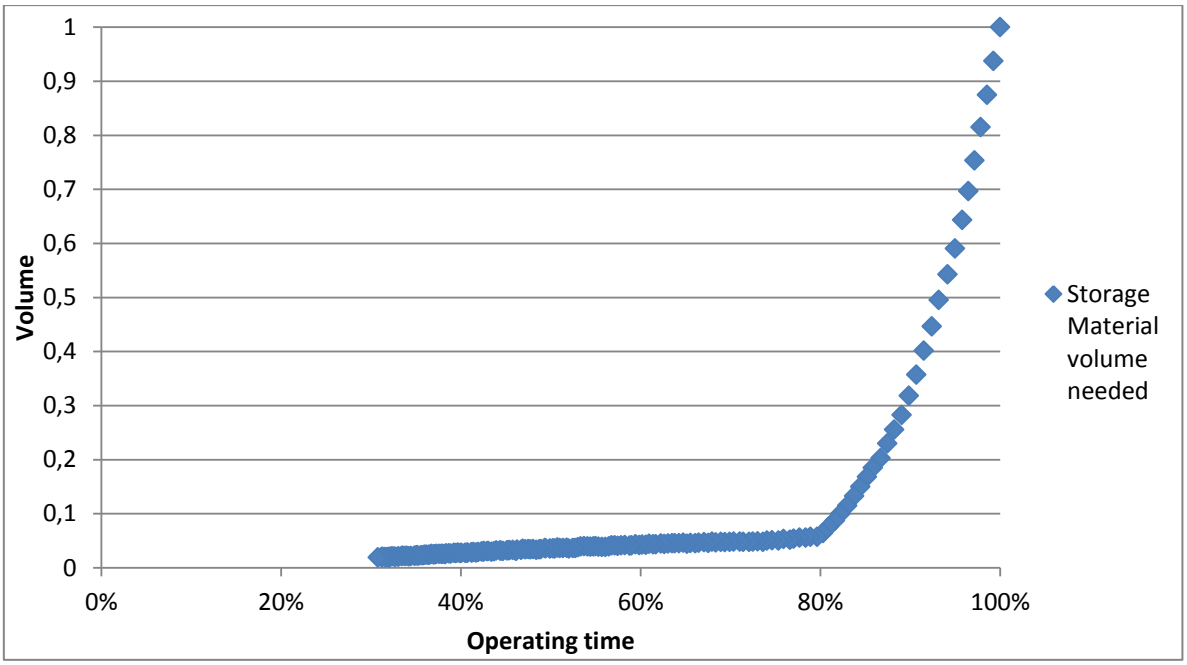

Fig. 20 - Relation between operating hours of the plant and storage material volume needed. Vertical axis is normalised.

The volume needed plotted in Fig. 20 does not include housing and insulation material. Part of the material is not heated up (during charging period) or cooled down (during discharging period) because the temperatures of the outlet cannot exceed the design parameters, extra volume should be considered when the system is implemented in the solar methane reforming plant.

4.6.1 Reference case

After evaluating the previous results a reference case to simulate the performance of the system should be set. The chosen case is the point immediately before the volume rises exponentially. In this case the plant does not operate for a low number of hours and the system is kept as small as possible. The reference case parameters are shown in Table 7.

Table 7 - Reference case parameters.

Reference case parameters	
Material mass density	2700 [kg.m-3]
Material heat capacity	0.88 [kJ.(kg-1.K-1)]
Temperature difference	532 [K]
Maximum energy Stored	889 [GJ]
Storage material volume needed	703.5 [m3]
Dimensions	≈8.9×8.9×8.9 m
Not operating hours	1785 [h]

When this approach is made it is necessary that the complete volume of the storage material changes its temperature (form 368 to 900 °C, in our application) and that it is no possible since the outlet temperature of the system cannot rise above the set parameters. It is necessary to increase the length of the system in order to keep the outlet temperature inside its boundaries values.

4.6.2 Charged and discharged gradients regarding extra length

The extra length needed to the system is determined by running a simulation under an “energy stored” condition. This condition stops the simulation when the maximum energy stored in the system is

achieved during charging period (to the maximum energy stored value it is summed the value of the energy stored in the system when it is fully discharged, since this energy will not be recovered from the system in order to guarantee that during discharging period the outlet temperature will not come below the temperature needed in the process). The simulation is run with a much higher length than the determined in the reference case. When this charged state is achieved, the system profile temperature is evaluated and the outlet is set where the material did not experience any temperature change. This guarantees that when the fully charged condition is achieved the outlet temperature does not exceed the minimum temperature of the process.

After the simulation, the total height of the system is determined. The dimensions of the system are showm in

Table 8 - System final dimensions.

Reference case parameters	
Cross section	≈8.9×8.9 m
Height	≈35m
Total volume	≈2772 [m3]

When the system is discharged the outlet temperature of the system cannot go below 900°C. In Fig. 21 is shown the discharged gradient of the system for the reference case, regarding the extra length needed to fulfill the required outlet temperature.

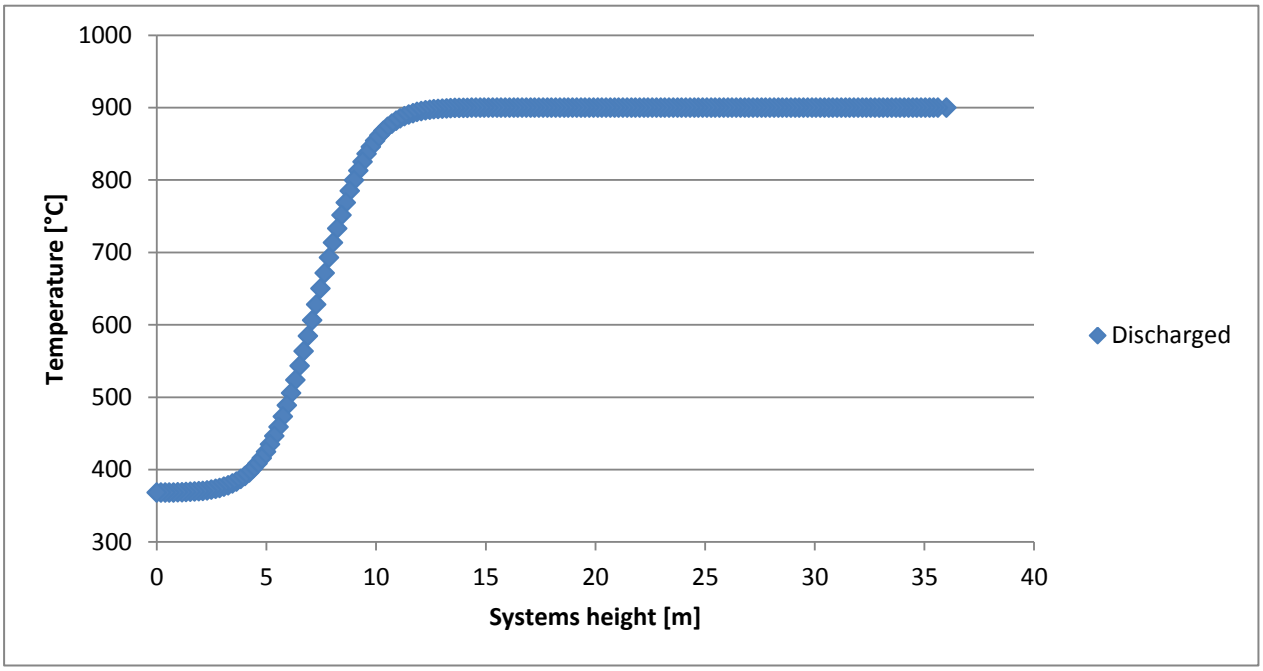

Fig. 21 - Reference case discharged temperature gradient considering extra length.

When the system is completely charged the outlet temperature of the system cannot rise above 368°C. In Fig. 22 is shown the charged gradient of the system for the reference case. The outlet during discharged is located on the left of the x axis (the flow is reversed when charging or discharging).

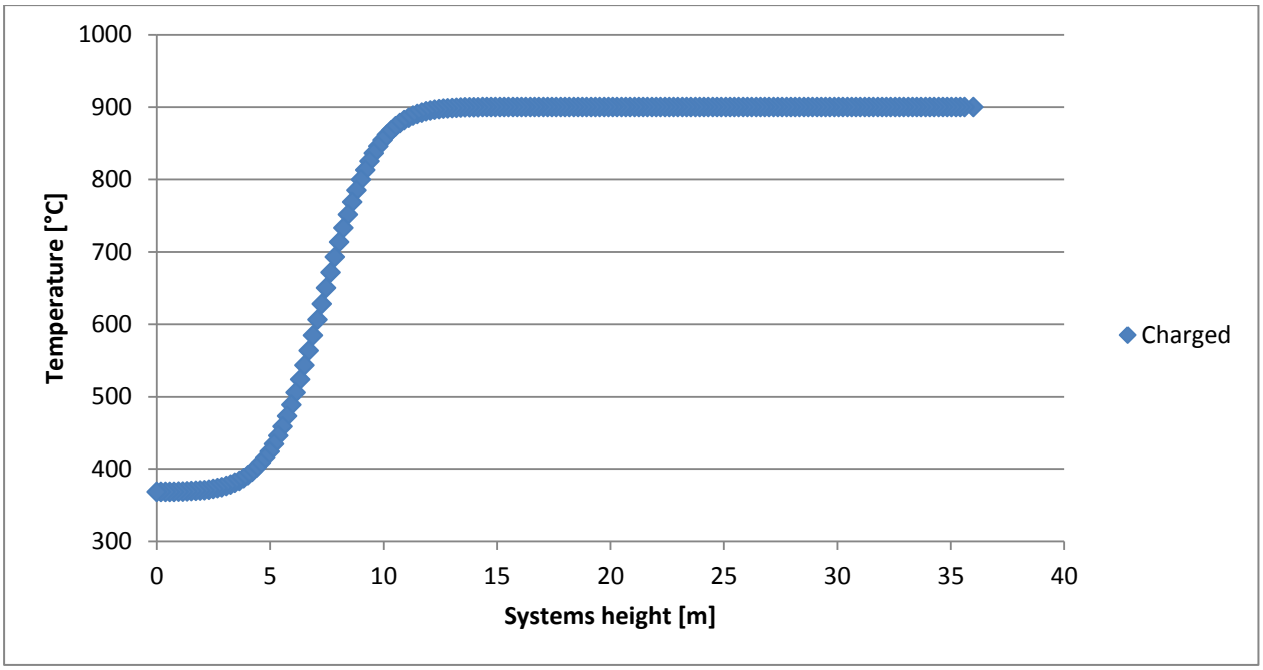

Fig. 22 - Reference case charged system temperature gradient considering extra length.

4.7 Reference case results

A simulation for the whole year will be carried out for the reference case system. An energy balance in the storage system was determined using an excel sheet and the first 8 hours of this energy balance are shown in Table 9. When the air to storage is a negative number means that the system is in discharging period. The values presented in Table 9 are results for the whole system.

The simulations results and the predicted values show a good agreement with a slight deviation that can be due to calculations approximation.

Table 9 - Simulations results for the first 8 hours of the whole year.

Hour	Intercepted Radiation [MWh]	Air flow to storage [kmol.h^{-1}]	Energy to storage [kJ.h^{-1}]	Energy accumulated in the storage [kJ]	Simulation energy accumulated results [kJ]	Error
1	32.98	1665.099758	28603849.58	28603849.58	28570513.3	0.12%
2	49.55	4752.74243	81644795.73	110248645.3	110120825.4	0.12%
3	52.5	5288.722731	90852111.88	201100757.2	200867525.1	0.12%
4	52.5	5288.722731	90852111.88	291952869.1	291614371.3	0.12%
5	52.5	5288.722731	90852111.88	382804981	382361310.1	0.12%
6	52.5	5288.722731	90852111.88	473657092.9	473108320.9	0.12%
7	41	3216.387444	55252583.05	528909675.9	528296684	0.12%
8	30.86	1299.706711	22326959.74	551236635.6	550597726.2	0.12%
9	0	29927.223	-50285183.22	500951452.4	500370168.2	0.12%

5. Conclusions

Energy storage will play a major role in the future of the solar technologies, when an energy storage system is available the utilization of these technologies will increase and will allow solar power to be produced on demand. Energy storage will allow a solar power plant to keep producing energy during cloudy periods or night period, when it is needed the most. And will increase the capacity factor of the plants without fossil fuel backup.

The main objective of this work was to model a high temperature heat storage system and predict its layout in order to overcome the intermittence of the sun as the energy source and to enable the operation of the plant under constant conditions. The type of system chosen to model was a sensible heat storage system due to the huge amount of information available about these systems.

The state of the art in thermal heat storage system is the two tank technology. Although, that technology did not fit to the reforming process due to the temperature boundaries related to the two tanks system.

The model was validated using data of previous works that modelled the same system. A simulation for the whole year will be carried out and for the first period of the simulation, the results of the system performance show an excellent agreement with the predicted values. The model can be easily adapted to other applications that want to make use of a sensible heat storage system, since the inputs and dimensions can be easily changed.

One major limitation of the model is the neglecting of thermal losses to the environment, even if those losses play a minor role in the system this losses can become an optimization work of the model in a near future. Also the degradation of the material after a long operating period should also be evaluated in the future, since these degradation can lead to thermophysical properties variation of the material.

An optimization of the model that can be carried out in the future is the determination of the housing and insulation material needed to install a complete system.

One of the main disadvantages of this system is the huge amount of area required to install it. Investigations in this field should be carried out in the future in order to reduce the volume of the system.

The major advantages of the system are its reliability and the fact that these system are close to other applications in industry which makes it an already known technology.

6. References

Abhat, A. (1983). "Low temperature latent heat thermal energy storage: heat storage materials." Solar Energy **30**(4): 313-332.

Agrafiotis, C., et al. (2014). "Exploitation of thermochemical cycles based on solid oxide redox systems for thermochemical storage of solar heat. Part 1: Testing of cobalt oxide-based powders." Solar Energy **102**: 189-211.

Agrafiotis, C., et al. (2014). "Solar thermal reforming of methane feedstocks for hydrogen and syngas production—A review." Renewable and Sustainable Energy Reviews **29**: 656-682.

Agrafiotis, C., et al. (2014). "Solar thermal reforming of methane feedstocks for hydrogen and syngas production - A review." Renewable and Sustainable Energy Reviews **29**: 656-682.

Bunsen Wong, L. B., Robert Buckingham, Dennis Thomey, Martin Roeb and Christian sattler (2013). Sulfur based thermochemical energy storage for concentrated solar power. SolarPACES2013 Conference.

Cárdenas, B. and N. León (2013). "High temperature latent heat thermal energy storage: Phase change materials, design considerations and performance enhancement techniques." Renewable and Sustainable Energy Reviews **27**(0): 724-737.

Coelho, B., et al. (2010). Solmass project–solar biomass dual hybrid 4 MW CRS pilot plant. SolarPACES Symposium, Perpignan.

Daschner, R., et al. (2013). "Pebble bed regenerator and storage system for high temperature use." Applied Energy **109**: 394-401.

Dunn, R. I., et al. (2012). "Molten-salt power towers: newly commercial concentrating solar storage." Proceedings of the IEEE **100**(2): 504-515.

European Academies Science Advisory Council (2011). Concentrating Solar Power: Its Potential Contribution to a Sustainable Energy Future. EASAC Policy Report 16, EASAC.

Gil, A., et al. (2010). "State of the art on high temperature thermal energy storage for power generation. Part 1—Concepts, materials and modellization." Renewable and Sustainable Energy Reviews **14**(1): 31-55.

Hasnain, S. (1998). "Review on sustainable thermal energy storage technologies, Part I: heat storage materials and techniques." Energy Conversion and Management **39**(11): 1127-1138.

Hirsch, T., et al. (2012). "DLR, Institute for Solar Research (DLR)."

Jegadheeswaran, S. and S. D. Pohekar (2009). "Performance enhancement in latent heat thermal storage system: a review." Renewable and Sustainable Energy Reviews **13**(9): 2225-2244.

Karagiannakis, G., et al. (2014). "Monolithic Ceramic Redox Materials for Thermochemical Heat Storage Applications in CSP Plants." Energy Procedia **49**: 820-829.

Khare, S., et al. (2013). "Selection of materials for high temperature sensible energy storage." Solar Energy Materials and Solar Cells **115**: 114-122.

Kolb, G. J. (2011). "Evaluation of annual performance of 2-tank and thermocline thermal storage systems for trough plants." Journal of Solar Energy Engineering **133**(3): 031023.

Kronhardt, V., et al. (2014). "High-Temperature Thermal Storage System for Solar Tower Power Plants with Open-Volumetric Air Receiver Simulation and Energy Balancing of a Discretized Model." Energy Procedia **49**: 870-877.

Laing, D. (2008). Solar thermal energy storage technologies. Energy Forum 10000 Solar Gigawatts, 23 April 2008.

Laing, D., et al. (2012). "High-temperature solid-media thermal energy storage for solar thermal power plants." Proceedings of the IEEE **100**(2): 516-524.

Laing, D., et al. (2008). "Solid media thermal storage development and analysis of modular storage operation concepts for parabolic trough power plants." Journal of Solar Energy Engineering **130**(1): 011006.

Lovegrove, K., et al. (1999). "A solar-driven ammonia-based thermochemical energy storage system." Solar Energy **67**(4): 309-316.

Luo, Z., et al. (2013). Simulation and Experimental Study on Long Term Sensible Thermal Energy Storage in Solar Thermal System. SolarPACES2013.

Michels, H. and R. Pitz-Paal (2007). "Cascaded latent heat storage for parabolic trough solar power plants." Solar Energy **81**(6): 829-837.

Miguel, S., et al. (2014). "100-Wh Multi-purpose Particle Reactor for Thermochemical Heat Storage in Concentrating Solar Power Plants." Energy Procedia **49**: 676-683.

Müller-Elvers, C., et al. (2012). "Design and Construction of Molten Salt Parabolic Trough HPS Project in Évora, Portugal." Proc. SolarPACES.

Müller-Steinhagen, H. and F. Trieb (2004). "Concentrating solar power." A review of the technology. Ingenia Inform QR Acad Eng **18**: 43-50.

Nagl, S., et al. (2011). The economic value of storage in renewable power systems-the case of thermal energy storage in concentrating solar plants, EWI Working Paper.

Nellis, G. and S. Klein Heat Transfer, Cambridge University Press.

Pitz-Paal, R., et al. (2013). "Solar Thermal Power Production." Transition to Renewable Energy Systems: 307-338.

Portaspana, J. C. (2011). MASTER THESIS High temperature thermal energy storage systems based on latent and thermo-chemical heat storage, Universität Wien.

Shah, R. K. and A. L. London (1978). Laminar flow forced convection in ducts: a source book for compact heat exchanger analytical data, Academic press.

Shukla, K. (1981). "Thermal energy storage for solar power generation: state of the art." Heat Transfer Engineering **3**(2): 62-72.

Steinmann, W.-D. and R. Tamme (2008). "Latent heat storage for solar steam systems." Journal of Solar Energy Engineering **130**(1): 011004.

Storch, H. V., et al. (2014). Investigation of Process Efficiency of an Indirectly Heated Solar Reformer, in: M. Eden, J.D. Siirola, G.P. Towler (Eds.). International Conference on Foundations of Computer Aided Process Design. WA,USA, Elsevier.

Tescari, S., et al. (2014). "Thermochemical Solar Energy Storage Via Redox Oxides: Materials and Reactor/Heat Exchanger Concepts." Energy Procedia **49**: 1034-1043.

Trieb, F., et al. (2014). "Concentrating solar power in a sustainable future electricity mix." Sustainability Science **9**(1): 47-60.

Tsoutsos, T., et al. (2005). "Environmental impacts from the solar energy technologies." Energy Policy **33**(3): 289-296.

Verdier, D., et al. (2014). "Experimentation of a High Temperature Thermal Energy Storage Prototype Using Phase Change Materials for the Thermal Protection of a Pressurized Air Solar Receiver." Energy Procedia **49**: 1044-1053.

Vogel, W. and H. Kalb (April 2010). Large-Scale Solar Thermal Power Technologies, Costs and Development.

Yang, J., et al. (2013). "Numerical analysis on the thermal behavior of high temperature latent heat thermal energy storage system." Solar Energy **98**: 543-552.

Yunus, A. C. and J. M. Cimbala (2006). "Fluid mechanics: fundamentals and applications." International Edition, McGraw Hill Publication: 185-201.

Zunft, S., et al. (2011). "Jülich Solar Power Tower—Experimental Evaluation of the Storage Subsystem and Performance Calculation." Journal of Solar Energy Engineering **133(**3): 031019.

Appendix A - Aspen Custom Modeler, Model Code

```
Model Storage_transient
  air as componentlistname (value: "air");
  air_in as input materialport (componentlist: air);
  air_cold as output materialport(componentlist: air);


//length domain
  ncells as coefficient(value: 450, spec:Fixed, lower: 1, upper: 500);
  L_hc as length (13; spec:fixed);
  x as lengthdomain (Length: L_hc, spacingPreference: 0.001, highestorderderivative: 2, Discretizationmethod:"BFD1");
  xnrange as integerset ([0:x.endnode]);

//energy balance variables

  T_air as Distribution1D (XDomain is x) of Temperature;
  T_w as Distribution1D (XDomain is x) of Temperature;

  q_overall as realvariable;

  q_w as Distribution1D (Xdomain is X, highestorderXderivative: 0) of realvariable (description:"Energy gain on the term");
  q_w_total as realvariable;

  Error as realvariable;


 //channel geometry
  s as length (5.2e-3, spec:fixed); //opening
  b as length (0.4e-3, spec:fixed); //thickness of struts

  A_cs_air as realvariable; //air channel cross section in m^2
  A_cs_air = s^2;
  A_cs_w as realvariable; // alumina cross section in m^2
  A_cs_w = ( (s+b)^2) - s^2;

 //Heat transfer coefficient auxiliar variables
//  Nu_hoff2(xnrange) as dimlessno;
  Re_w(xnrange) as dimlessno;
  Pr(xnrange) as dimlessno;
  alpha_hoff2(xnrange) as heat_trans_coeff (upper:30000); //in W/m²/K
  Nusselt as dimlessno (spec:fixed, value:3.61);


//air properties
  mu_air(xnrange) as viscosity (Description:"viscosity of air, in cP!!");
  rho_air(xnrange) as dens_mol (Description:"density of air, molar"); //kmol/m³
  rho_air_m(xnrange) as dens_mass (Description:"density of air, mass"); //kg/m³
  M_air as molweight;
  call(M_air) = pmolweight(air_in.z) air_in.componentlist;
  c_air(xnrange) as cp_mol; // in kJ/kmol/K
  lambda_air(xnrange) as conductivity; //in W/m/K
  u_air(xnrange) as velocity(upper: 10e6);
  n_air as realvariable; //air molar flow in kmol/s
  n_air = air_in.F/3.6;
  h_air (xnrange) as enth_mol;

//alumina properties
  cp_alumin as realparameter (value: 0.88); //cp mean of alumina kJ/kg/K
  rho_alumin_m as realparameter (value: 2700); //alumina mass density kg/m^3
  lambda_w as conductivity (spec:fixed, value: 2.1); //in W/m/K

//pressure drop
  p_cell(xnrange) as pressure;
  p_drop (xnrange) as realvariable; //pressure drop between two consecutive cells [bar]
  f (xnrange) as realvariable; //friction factor
  g as realvariable (spec:fixed, value:9.80665); //Gravitational acceleration [m/s^2]
  p_tot as realvariable;
```

```
  for i in xnrange do

  call(rho_air(i)) = pDens_mol_vap (T_air(i),p_cell(i), air_in.z) air_in.componentlist; // air molar density [kmol/m^3]
  call(c_air(i)) = pCp_mol_vap(T_air(i) ,p_cell(i),air_in.z) air_in.componentlist; // air heat capacity [kJ/kmol/k]
  call(mu_air(i)) = pVisc_vap(T_air(i),p_cell(i), air_in.z) air_in.componentlist; // air viscosity [cP]
  call(rho_air_m(i)) = pDens_mass_Vap (T_air(i), p_cell(i), air_in.z) air_in.componentlist; // air density [kg/m^3]
  call(lambda_air(i)) = pCond_Vap(T_air(i),p_cell(i),air_in.z)air_in.componentlist; //air conductivity [W/m/K]
  call(h_air(i))=pEnth_mol(T_air(i),p_cell(i),air_in.z)air_in.componentlist; //air molar enthalpy [GJ/kmol]

  Re_w(i)*mu_air(i)*1e-3 = u_air(i)* s *rho_air_m(i);

  Pr(i)*M_air*lambda_air(i)= mu_air(i)*1e-3* c_air(i)*1e3;

  //Nu_hoff2 (i) = 0.8114 * (3.66^2 + 0.7^3 + (1.615 * (Re_w(i)* Pr(i) * (s/L_hc))^(1/3) - 0.7)^3)^(1/3);
  Nusselt * lambda_air(i) = alpha_hoff2(i) * s;

  f(i) = 56.92/(Re_w(i) );

  u_air(i)*(rho_air(i)*s^2) = n_air/1e3;

  $q_w.value(i) = ( rho_alumin_m * cp_alumin * A_cs_w * x.section(1).spacingUsed* $T_w.value(i) )* 1000;

endfor

for i in x.interior do

  p_cell(i) = p_cell(i-1)-p_drop(i);
  p_drop(i) = (((f(i) * ((x.section(1).spacingUsed)/s)*(rho_air_m(i)*u_air(i)^2)/2) + rho_air_m(i) * g * x.section(1).spacingUsed)/1e5);

  (n_air/1e3)* (((h_air(i)-h_air(i-1))*1e9)/(x.section(1).spacingUsed)) + (rho_air(i) * c_air(i) * A_cs_air * $T_air(i)) * 1000 =
  -4* alpha_hoff2(i) * s *(T_air.value(i) - T_w.value(i)) ; // in W/m

  (rho_alumin_m * cp_alumin * A_cs_w * $T_w(i) ) * 1000 = 4* alpha_hoff2(i) * s *(T_air.value(i) - T_w.value(i))  + A_cs_w* lambda_w*T_w(i).d2dx2;

endfor
for i in x.interior do

  p_cell(i) = p_cell(i-1)-p_drop(i);
  p_drop(i) = (((f(i) * ((x.section(1).spacingUsed)/s)*(rho_air_m(i)*u_air(i)^2)/2) + rho_air_m(i) * g * x.section(1).spacingUsed)/1e5);

  (n_air/1e3)* (((h_air(i)-h_air(i-1))*1e9)/(x.section(1).spacingUsed)) + (rho_air(i) * c_air(i) * A_cs_air * $T_air(i)) * 1000 =
  -4* alpha_hoff2(i) * s *(T_air.value(i) - T_w.value(i)) ; // in W/m

  (rho_alumin_m * cp_alumin * A_cs_w * $T_w(i) ) * 1000 = 4* alpha_hoff2(i) * s *(T_air.value(i) - T_w.value(i))  + A_cs_w* lambda_w*T_w(i).d2dx2;

endfor

  //energy balance
  q_overall:0,initial;
  $q_overall = ((n_air/1e3)* ((h_air(x.endnode)-h_air(0))*1e9));

  if q_overall==0 then
  Error = 0;
  else
  Error = ((q_overall+q_w_total)/(q_overall))*100;
  endif



  q_w:0,initial;
  q_w_total:0,initial;
  q_w_total = sigma(q_w.value([xnrange]));

  //pressure drop
  p_tot = sigma(p_drop);

 //air initial conditions
  T_air( x.interior + x.endnode) : 368,initial;

 //wall initial conditions
  T w ([0:x.endnode]): 368,initial;

 //inlet boundary conditions
  p_drop(0) = 0;
  p_cell(0) = air_in.p;
  T_air(0)=air_in.T;
  (rho_alumin_m * cp_alumin * A_cs_w * $T_w(0) ) * 1000 =
  4* alpha_hoff2(0) * s *(T_air.value(0) - T_w.value(0))  + A_cs_w* lambda_w*(T_w(0).ddx/x.section(1).spacingUsed);


 //outlet boundary conditions

  p_cell(x.endnode) = p_cell(x.endnode-1)-p_drop(x.endnode);
  p_drop(x.endnode) = 0;
  (rho_alumin_m * cp_alumin * A_cs_w * $T_w(x.endnode) ) * 1000 =
  4* alpha_hoff2(x.endnode) * s *(T_air.value(x.endnode) - T_w.value(x.endnode))  - A_cs_w* lambda_w*(T_w(x.endnode).ddx/x.section(1).spacingUsed);

  (n_air/1e3)* (((h_air(x.endnode)-h_air(x.endnode-1))*1e9)/(x.section(1).spacingUsed)) + (rho_air(x.endnode) *
  c_air(x.endnode) * A_cs_air * $T_air(x.endnode)) * 1000 = -4* alpha_hoff2(x.endnode) * s *(T_air.value(x.endnode) - T_w.value(x.endnode));

 //Set output parameters.
  air_cold.T = T_air(x.endnode);
  air_cold.p = p_cell(x.endnode);
  air_cold.z(air) = air_in.z(air) ;
  call(air_cold.h) = pEnth_mol_Vap(T_air(x.endnode), p_cell(x.endnode), air_in.z)air_in.componentlist;
  air_cold.Av = Air_in.Av;
  air_cold.F = air_in.F;
  air_cold.V*rho_air(x.endnode) = 1;


End
```

Appendix B - Hourly intercept radiation and correspondent air mass flow

Hour	Qic (MHh MHh.12000)	Hour	Qic (MHh.12000)	Hour	Qic (MHh MHh.12000)
1	32,98	19	0	41	0
2	49,55	20	0	42	0
3	52,5	21	0	43	0
4	52,5	22	0	44	0
5	52,5	23	0	45	0
6	52,5	24	8,02	46	0
7	41	25	33,27	47	0
8	30,86	26	52,13	48	9,42
9	0	27	52,5	49	38,24
10	0	28	52,5	50	52,5
11	0	29	52,5	51	52,5
12	0	30	52,5	52	52,5
13	0	31	44,98	53	52,08
14	0	32	22,37	54	51,08
15	0	33	0	55	44,16
16	0	34	0	56	26,42
17	0	35	0	57	0
18	0	36	0	58	0